

Optimisation of confinement in a fusion reactor using a nonlinear turbulence model

E. G. Highcock^{1,2,3,†}, N. R. Mandell⁴, M. Barnes², and W. Dorland⁵

¹Department of Physics, Chalmers University of Technology, Gothenburg, Sweden

²Rudolph Peierls Centre for Theoretical Physics, 1 Keble Road, Oxford, UK

³Culham Centre for Fusion Energy, Culham Science Centre, Abingdon, UK

⁴Department of Astrophysical Sciences, Princeton University, Princeton, New Jersey, USA

⁵Department of Physics, University of Maryland, College Park, Maryland, USA

(Received xx; revised xx; accepted xx)

The confinement of heat in the core of a magnetic fusion reactor is optimised using a multidimensional optimisation algorithm. For the first time in such a study, the loss of heat due to turbulence is modelled at every stage using first-principles nonlinear simulations which accurately capture the turbulent cascade and large-scale zonal flows. The simulations utilise a novel approach, with gyrofluid treatment of the small-scale drift waves and gyrokinetic treatment of the large-scale zonal flows. A simple near-circular equilibrium with standard parameters is chosen as the initial condition. The figure of merit, fusion power per unit volume, is calculated, and then two control parameters, the elongation and triangularity of the outer flux surface, are varied, with the algorithm seeking to optimise the chosen figure of merit. A two-fold increase in the plasma power per unit volume is achieved by moving to higher elongation and strongly negative triangularity.

1. Introduction

Convective heat loss resulting from micro-turbulent fluctuations in a fusion reactor limits the ability of such a reactor to confine heat to the degree required to achieve fusion. Above some critical temperature gradient, this heat loss rises extremely rapidly, limiting the central temperature and hence the fusion reaction rate. Empirically, one way to improve fusion performance despite this obstacle is to build larger devices.† Current planning for the first demonstration power plant (Federici *et al.* 2014) envisions a device more than 20 times larger by volume than the world's largest operating test reactor, the Joint European Torus (JET). Such a tactic remains the surest route to achieving fusion with our current understanding. However, the approach is not without difficulties. First, the individual cost of such a large plant is very high (although the power output scales accordingly), putting the construction of such reactors, as well as necessary precursor experiments and test reactors, out of the reach of all but major governments. Second, the larger designs place much greater demands upon the construction materials (see e.g. the discussion in Stork *et al.* (2014)).

The reactor design effort is constantly finding innovative ways to mitigate these

† Email address for correspondence: highcock@chalmers.se

† This is based on the observation that the global confinement of heat improves with size (EJ Doyle *et al.* 2007), which is believed to stem from the corresponding increase in the height of the spontaneously-formed transport barrier which forms at the edge of the plasma in typical conditions (see e.g. Maggi *et al.* 2007).

problems. For example, one approach to achieving more compact and cost-effective designs is to use new high-temperature superconductors which have lower cost and greater tensile strength than the superconductors used today, and which can be constructed so as to allow easy disassembly for maintenance (Sorbom *et al.* 2015).

However, while such approaches have frequently used state of the art modelling for almost all of the construction of the reactor, none of these studies have incorporated the turbulent heat loss using nonlinear models which accurately capture the essential properties of the turbulence. Instead, the vast majority use scaling laws, either inspired by dimensional arguments or extrapolated from current experiments (Uckan 1990; Galambos *et al.* 1995; Luce *et al.* 2014; Sorbom *et al.* 2015) (see also discussion in Zohm *et al.* (2013)). It is also possible to use more sophisticated “quasilinear” models (Staebler *et al.* 2007; Bourdelle *et al.* 2016) which calculate the linear properties of the instabilities which drive the turbulence and use phenomenological rules, and calibration to a pre-determined subset of nonlinear simulations, to calculate the turbulent heat loss from these linear properties. Use of these quasilinear models includes both full reactor design studies (e.g. Staebler & John (2006); Wenninger *et al.* (2015); Jardin *et al.* (2006)) and efforts to predict and optimise performance for particular devices (e.g. Mukhovatov *et al.* (2003); Budny (2009); Kinsey *et al.* (2011); Parail *et al.* (2013); Meneghini *et al.* (2016)). Additionally, there have been advances in using neural-network approaches to allow such methods to fully replace the simple scaling laws by facilitating extremely fast simulation based on the quasilinear models (Citrin *et al.* 2015*a*). Nonetheless, nonlinear turbulence calculations, while used routinely for investigation of individual experiments and verification of quasilinear models, have been conspicuously absent from reactor design.†

The primary reason for the absence of nonlinear models is their cost and complexity. Effectively, it would have been impossible until recently to have completed a design study including these models on any reasonable timescale. This absence represents a missed opportunity. Over the last 20 years there has been a great increase in understanding, derived from both experiment and theoretical inquiry, of the circumstances in which the levels of turbulence can be greatly reduced, without reducing the temperature gradient (Burrell 1997; Synakowski 1999; Highcock *et al.* 2010; Barnes *et al.* 2011*a*; Highcock *et al.* 2012; Citrin *et al.* 2015*b*). Such effects can be, and have been, included in quasilinear and other models *a posteriori*. However, even where designs are based on extrapolation from the best performing experimental configurations, using the most complete reduced models available at the time (e.g. Jardin *et al.* (2006)), the designs can know nothing of potential new phenomena, leading to possible further gains, that might exist in the vast configuration space at their disposal (more than two decades ago, Galambos *et al.* (1995) showed that in theory, where full control could be maintained over turbulent transport, it was possible to reduce the capital cost of the reactor plant by 30%, that is, 10 billion (1995) US dollars, compared to the most advanced designs of the day). This still-largely-uncharted configuration space is best explored in conjunction with nonlinear models, since any exploration by reduced models could conceivably miss a crucial physics effect not yet included within the model‡ (c.f work in the stellarator community which clearly

† In stating this we have not overlooked the important work across the entire field (which a lack of space prevents us from surveying) studying the performance of and possible improvements to *existing* designs such as ITER and DEMO using nonlinear simulations. It is the success of such work that motivates inclusion of nonlinear analysis in the design process itself.

‡ As discussed in more detail below, this proof-of-principle study includes only an electrostatic, adiabatic-electron, hybrid gyrofluid-gyrokinetic nonlinear model, but the

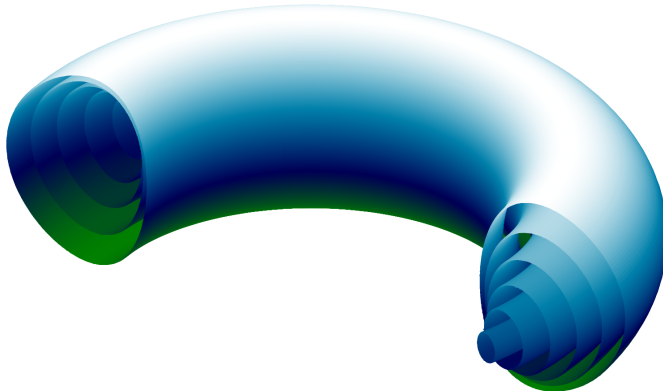


FIGURE 1. An illustration of the nested magnetic flux surfaces that confine a fusion plasma. The shape of these fluxes corresponds to the initial shape used for this study.

demonstrates the benefit of tight integration of stellarator optimisation with nonlinear analysis; Xanthopoulos *et al.* (2014)).

Every fusion experiment costs a vast sum to build, and owing to the hard limits placed by all components of the reactor, can only explore a certain small region of the high- (or infinite-) dimensional design space. It is beholden upon theory and numerical study to search the design space, at several-orders-of-magnitude smaller expense, to identify the most promising regions. However, in order for this search to be meaningful, we must have confidence in the predictions. The simplified models used must either be pessimistic, or be used only in regimes where they have been benchmarked against more complete models or experiment and thus preclude the possibility of entirely new design paradigms. By contrast, careful comparison with experiment over recent years has provided a high degree of confidence that nonlinear models (specifically gyrokinetic models, which use a five-dimensional reduction of the Vlasov equation valid in the conditions of a fusion reactor; for a review see Abel *et al.* (2013)), without any provision of tuning or fitting parameters, are able to accurately predict what the properties of turbulence will be like in a given situation (White *et al.* 2013; Citrin *et al.* 2014; van Wyk *et al.* 2016).

2. A first-principles model

Here we present the first case where a first-principles nonlinear model of turbulence (specifically a novel hybrid gyrofluid/gyrokinetic model, described below, which produces excellent agreement with gyrokinetic models) has been used, as part of a multi-scale transport analysis, to calculate the performance of the core of a given configuration *ab initio* and then seek for a higher performing solution. In this particular study, the optimisation algorithm chosen achieved an improvement in the fusion power per unit volume of 91%. However, this first study is envisioned as a proof of concept, as the stepping stone for a much larger effort in which many more dimensions of parameter space are explored.

A magnetic fusion reactor is composed of a plasma confined by a series of nested toroidal magnetic flux surfaces (Fig. 1). The plasma is composed of ionised deuterium and tritium, which fuse together to produce helium, neutrons, and a large amount of energy, provided sufficient pressure is achieved over sufficient volume in the centre of

methodology demonstrated is already capable of being extended to include a full gyrokinetic electromagnetic multi-species calculation, albeit at increased cost.

the plasma. The magnetic field is provided by a series of large external field coils and a current which flows through the plasma itself (as well as by various small coils responsible in addition for the stability of the field). The plasma is heated in a number of different ways: by the current itself, by the injection of a beam of high energy neutral particles, and by high power electromagnetic radiation of various frequencies. Fuel is injected by means of puffs of gas, frozen pellets, and neutral particle beams. Heat is lost via neutrons, radiation and by particle loss to the wall (which is concentrated in a special target region called the divertor). In this investigation we consider the core of the reactor; that is we consider the inner $\sim 90\%$ (by minor radius) of the flux surfaces. We assume the existence of an edge transport barrier, that is, that there is good confinement with a steep pressure gradient in the remaining $\sim 10\%$ of the plasma (a standard assumption since the discovery of the “high-confinement mode”; Wagner *et al.* (1984)). We also assume that the barrier is independent of elongation and triangularity (this assumption, necessary because we are considering only core transport, differs from current experimental observations, and is discussed further below).

The software used in this study to optimise such a reactor is the CODERUNNER Fusion Optimisation Framework (CORFU). This is a sizeable edifice of software comprising many independent parts, as illustrated in Fig. 2. The equations underlying the framework are given in Appendices A–D. The calculation proceeds as follows.

To begin with, the choice of optimisation control parameters, and all other requisite input information, is provided to the CORFU framework, which acts as the optimisation driver. From this input, an initial configuration is assembled, comprising parameterisations of:

- the shape of the flux surface at the edge of the plasma core;
- the profile of the toroidal current, and
- the initial pressure profile, including a fixed finite pressure at the edge of the plasma core.

These are used (Link 1 in Fig. 2) by the CHEASE code (Lütjens *et al.* 1996) to calculate the shape of the magnetic flux surfaces (i.e., the equilibrium magnetic field).

For the initial configuration we consider a *purely hypothetical* tokamak. We do, however, choose machine parameters (see Table 1) that are comparable in magnitude to those of a large tokamak—the Joint European Torus (JET)—and profiles that are plausible for such a tokamak (Fig. 5; see e.g. Barnes *et al.* (2011a) or the tokamak profile database described in Roach *et al.* (2008) for a comparison).

The initial configuration, including the magnetic equilibrium solution, details of external heat sources and the profiles of particle density (densities and external sources are held fixed) are then used (Links 2 and 3) by the TRINITY transport solver (Barnes *et al.* 2010) to find the pressure (and thus the fusion power generated), across the whole of the plasma, with the additional assumption that the temperatures of the ions and electrons are kept equal by collisional equilibration.† This is done by allowing the pressure profile to evolve until the heat losses, due to turbulence (discussed below) and other effects (in this study, neoclassical transport and radiative losses, see Appendix A), match the heat inputs, both external and that generated by fusion. However, since the magnetic equilibrium itself is affected by the pressure, the result of the TRINITY calculation must be fed back to CHEASE (Link 4), a new equilibrium generated, and TRINITY rerun, until the cycle converges, the pressure stops changing and a steady-state solution is found.

† This limits the possibility of interplay between the electron and ion heating and loss channels, either to good or ill; we note again that this and other limitations of this proof-of-principles study are discussed more fully below.

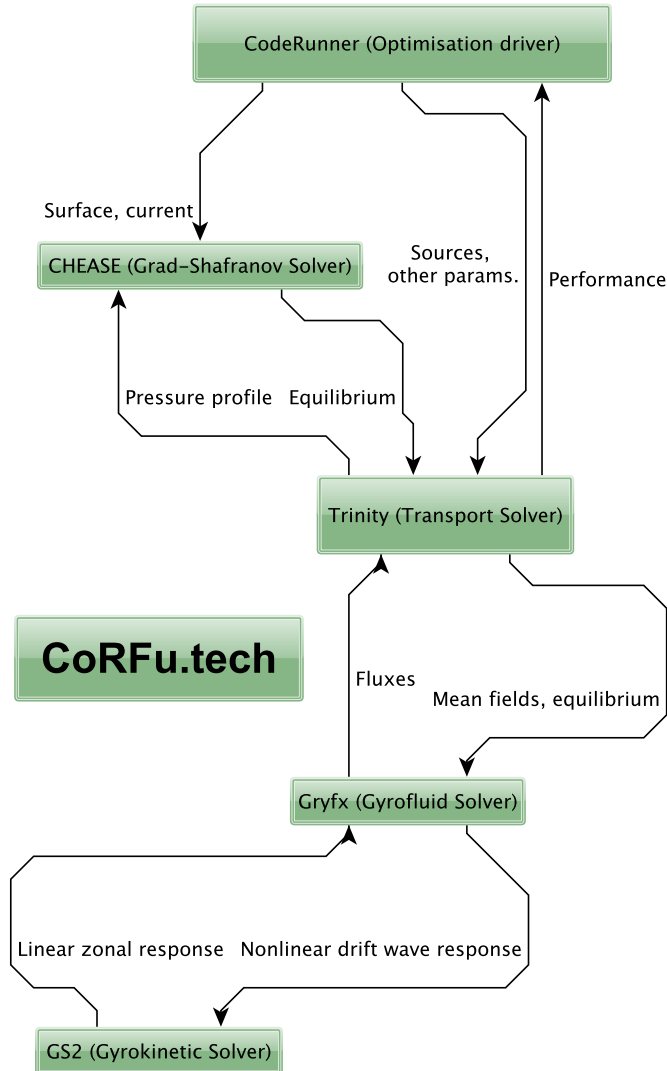


FIGURE 2. Schematic of the CORFU framework.

To calculate the heat loss due to turbulence (Links 5 and 8), TRINITY uses several simultaneous copies of the GPU-based hybrid gyrofluid/gyrokinetic code GRYFX (see Appendices B–D). Each copy of GRYFX calculates the heat flux resulting from the turbulence at a particular location in the plasma, that is, on a particular magnetic flux surface, given the pressure profile and magnetic equilibrium. A mean-field, multi-scale approach is used. The turbulent heat flux is calculated for the current pressure profile; the heat flux is then used to evolve the pressure profile, at which point the turbulent heat flux is recalculated. An illustration of the complete system is given in Fig. 3.

The GRYFX code divides the calculation of the heat flux in two (Links 6 and 7) using a novel algorithm: the evolution of the smaller scale drift waves is calculated using the gyrofluid model (Dorland & Hammett 1993; Beer & Hammett 1996) by GRYFX, and the evolution of the large-scale zonal flows which are generated by the turbulence is calculated by the gyrokinetic code GS2 (Dorland *et al.* 2000; Kotschenreuther *et al.* 1995), with the nonlinear interaction between the two scales (and among the drift waves of various scales)

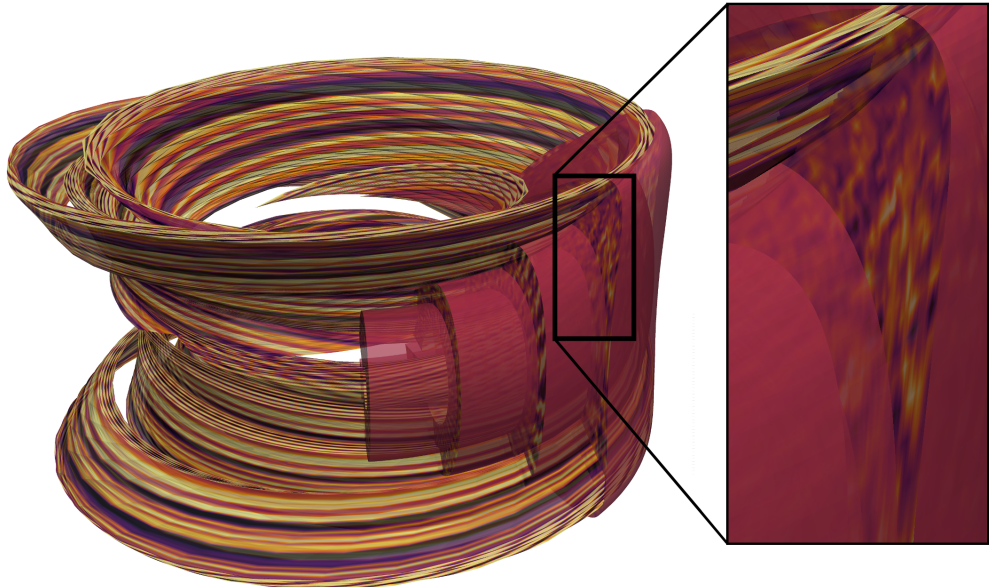


FIGURE 3. An illustration of a TRINITY simulation showing above-threshold turbulence for the optimal configuration. The elongated ribbons to the left of the main picture are flux tubes (Beer *et al.* 1995), the domains in which the turbulence is calculated, using the local approximation which assumes the turbulent fluctuations are small-scale perpendicular to the magnetic field. Assuming statistical periodicity (which again results from the small scale of the fluctuations), these flux tubes can be repeated to fill the four flux surfaces being simulated (which are shown cut away to the right of the main picture). The picture to the right shows the cross-section of the turbulence.

being calculated in GRYFX (see Appendix D). The simulations are electrostatic with a Boltzmann response for electrons.

The transport calculation within TRINITY used only five radial grid points. This was to reduce the overall cost of this first study, and would be increased in future work. Nonetheless, we note that the 5-point derivative stencil used radially by Trinity, and the fact that the transport calculations evolved to steady state (where power balance was satisfied on each flux surface), will reduce the impact of the sparse radial grid on the results of this study.

3. Finding the optimal solution

When the pressure, magnetic equilibrium, and turbulent heat fluxes have ceased to evolve, a steady-state solution has been found. At this point, the figure of merit for this solution (the fusion power per unit volume) is used by the optimisation driver CODERUNNER (Link 9 in Fig. 2), to generate a new set of control parameters according to the particular optimisation algorithm being used. In this study, the Nelder-Mead simplex algorithm was selected[†] (not to be confused with the simplex algorithm in linear

[†] The simplex algorithm was chosen for its reliability in this initial study. However, the CORFU framework is expected to be used to explore a multi-dimensional design space with a plethora of local maxima. This next step will first require a careful study of the suitability of various multi-dimensional optimisation algorithms both standard and novel, whether heuristics like simulated annealing or genetic algorithms, and whether gradient-free like Nelder-Mead, or pseudo-gradient like BFGS and variants. Lewis (2004) provides a good

programming). This is a slow but robust algorithm that constructs a simplex with $N+1$ vertices in an N -dimensional configuration space and then at each stage takes the “worst” vertex and moves it to a more optimal place. Visually, one can perceive the simplex “crawling uphill” (Fig. 4).

Using the new values of the control parameters provided by the simplex algorithm (i.e. the next “guess”) the whole of the previous cycle is repeated, determining the figure of merit for this next configuration. The calculation proceeds likewise until it has converged on a maximum to within some specified tolerance (or until a prescribed number of iterations have taken place).

The two control parameters chosen were the elongation and triangularity of the outer flux surface (as defined in Lütjens *et al.* (1996)). The shape of the magnetic field has long been known to have a marked effect on the turbulence, and the choice of these two shaping parameters in particular was motivated by pioneering experimental work on the TCV tokamak, which was designed to allow large variation in both—demonstrating a consequent large variation in performance (Weisen *et al.* 1999).

The results are displayed at the bottom of Fig. 4. In this figure one can observe the evolution of the control parameters, starting with three initial guesses of $(\kappa, \delta) = (1.3, 0.2)$, $(1.3, 0.1)$ and $(1.4, 0.1)$. The lowest initial vertex is $(1.3, 0.2)$ with a power per unit volume (P/V) of 0.0313 MW m^{-3} . Initially the algorithm moves to higher elongation and lower triangularity, before proceeding to keep elongation roughly constant and to continue to decrease triangularity. The iteration was terminated when values of triangularity moved significantly beyond the limits of what has been seen in experiment (~ 0.65 Pocheleon *et al.* (1999)). The final, optimal value of P/V of 0.0598 MW m^{-3} with $(\kappa, \delta) = (1.6, -0.625)$. Thus, an improvement of 91% was discovered over the course of the optimisation. Since the final value of triangularity was somewhat extreme, we also provide data for an intermediate result with $(\kappa, \delta) = (1.525, -0.25)$, for which P/V is 0.0481 MW m^{-3} .

It is interesting also to consider the evolution of the confinement time, defined as the total amount of stored kinetic energy divided by the rate of energy injection, is displayed in Fig. 6. We also see that optimising the confinement time, which reflects the ability of the system to confine heat, would have produced different results to optimising the fusion power per unit volume; in particular, the improvement at negative triangularity is less marked, and moving to higher elongation at positive triangularity may have produced a similar improvement in the confinement time.

4. Discussion and Outlook

It has been shown that, without any tuning of model parameters, it has been possible to generate a plausible solution for reactor performance and then optimise it. The final fusion power in this study is small compared to the input heating power (on the ions) of 20MW, but that is because the parameters in this study (Tab. 1) are not reactor-like, but rather of the same order of magnitude as those of JET, the largest existing device: a choice made to allow assessment of the credibility of the initial solution. Even more encouragingly, the qualitative result of this optimisation—that core confinement improved at lower triangularity and higher elongation—is directly

overview. The field of nonlinear multi-dimensional optimisation is large and increasing, with both commercial (ESTECO 2018) and freely available Abramson *et al.* (2006) software offerings. Wide, too, is the literature on the comparison of algorithms, whether individual examples (Manousopoulos & Michalopoulos 2009) or more abstract papers investigating the techniques of algorithm comparison, or metamodeling (Simpson *et al.* 2008).

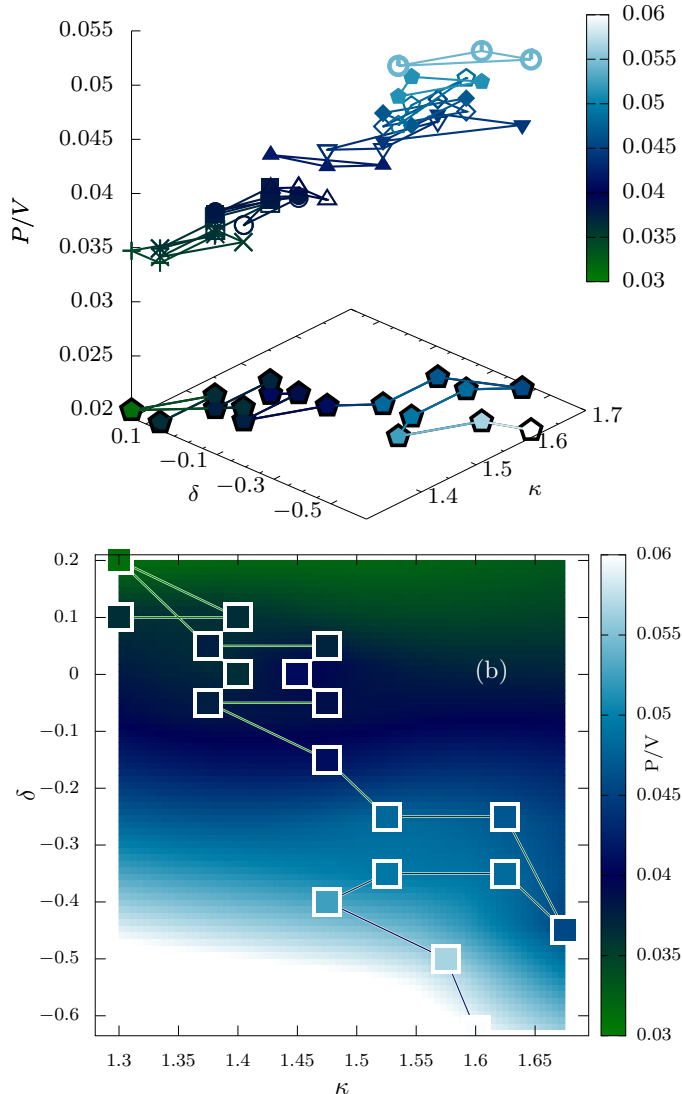


FIGURE 4. *Top.* Diagram illustrating the search path taken by the simplex optimisation algorithm. The suspended triangles represent the simplex at each iteration, with the colour and height of each triangle equal to the average of the values of P/V at each of the vertices. The curve in the base plane indicates the actual sequence of function calls, that is, the actual sequence of (κ, δ) values evaluated by TRINITY. *Bottom.* P/V as a function of κ and δ , both the function values (squares) and an interpolated surface, with the colour being the value of P/V . The highest (optimal) value is at $\kappa = 1.60$, $\delta = -0.625$. An intermediate solution, with a triangularity within the bounds of what has currently been realised, is chosen at $\kappa = 1.525$, $\delta = -0.25$.

corroborated by experimental measurements on the TCV tokamak (Weisen *et al.* 1999) and theoretical studies (Marinoni *et al.* 2009), although as TCV is a much smaller device than that we consider here, with important effects arising from kinetic electron modes and finite gyroradius, quantitative comparisons cannot be justified.

The challenges inherent to this study, and the obstacles to such a study being carried out in the past, proceed principally from the calculation of the turbulent fluxes. All in

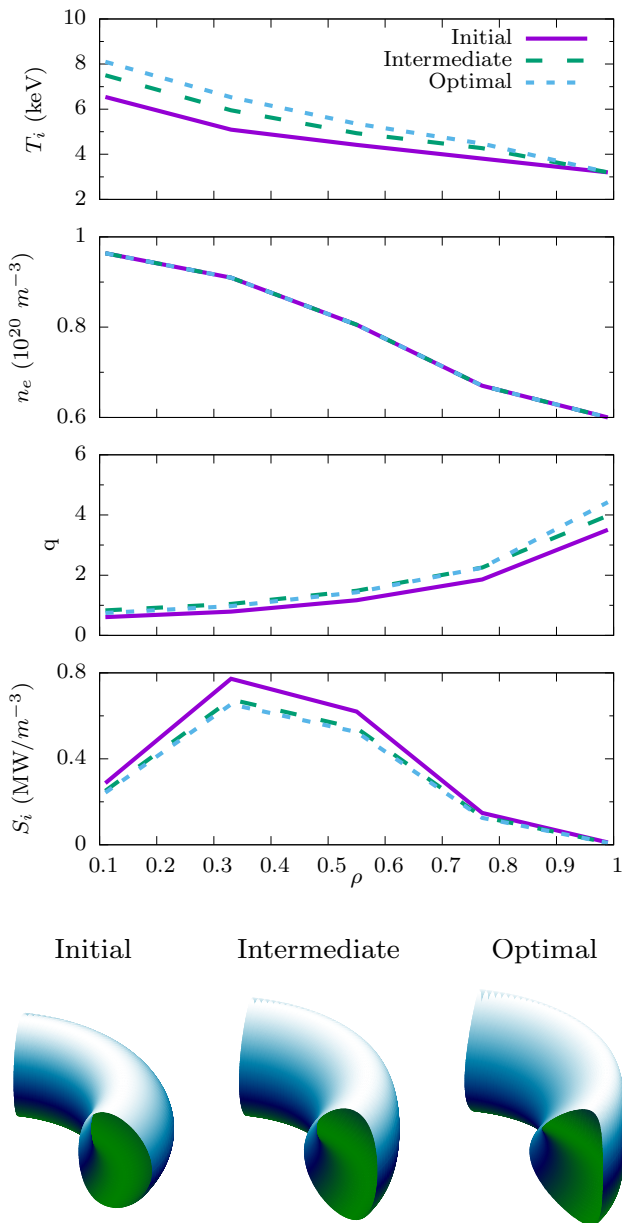


FIGURE 5. *Top.* Profiles of ion temperature (T_i), electron density (n_e), safety factor (q) and heat input (S_i), showing the values of each quantity versus normalised radius ρ . ρ is a dimensionless quantity which labels the flux surface. In this work we examine core transport; thus at the outer flux surface ($\rho = 1$) there is a finite temperature of 3.2 keV and a finite electron density of $0.6 \times 10^{20} \text{ m}^{-3}$. *Bottom.* Outer flux surface shapes of the initial, intermediate and optimal solutions.

all a total of 8680 converged nonlinear turbulence calculations at a spatial resolution of $192 \times 96 \times 20$ (radial \times poloidal \times parallel) were required, at a total cost of approximately 3000 GPU-accelerated node hours. That such an exercise was possible was owing to two developments. The first was the design of the implicit algorithm in the TRINITY code which reduced the number of turbulence calculations required (Barnes *et al.* 2010). The

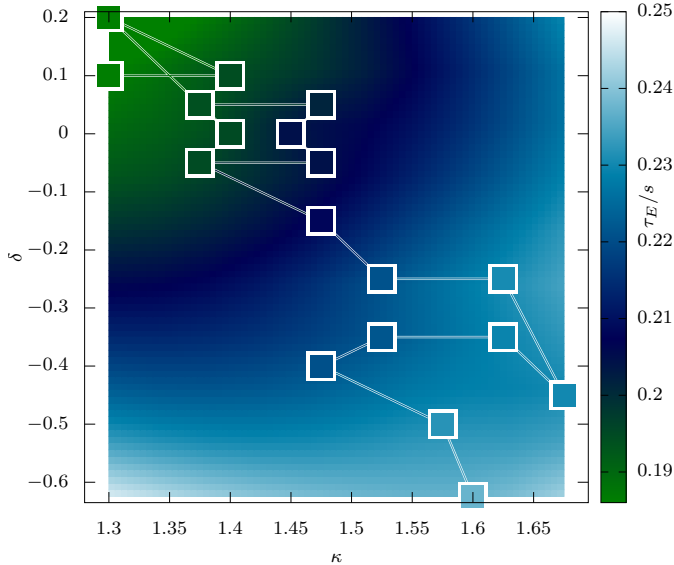


FIGURE 6. Evolution of the confinement time in seconds, given as a function of elongation κ and triangularity δ . Squares represent data points, shown on top of an interpolated surface for illustration of the overall trend.

	Initial	Intermediate	Optimal
On-axis Magnetic Field. (T)	2.91	2.84	2.81
On-axis Major Radius (m)	3.12	3.17	3.21
Ion input heat S_i (MW)	20	20	20
Plasma current I_p (MA)	1.9	1.9	1.9
Elongation κ	1.3	1.525	1.60
Triangularity δ	0.2	-0.25	-0.625
Core Volume V (m ³)	59.3	67.1	71.8
Confinement time (s)	0.179	0.221	0.237
Fusion Power P (MW)	1.85	3.23	4.30
P/V (MW/m ³)	0.0313	0.0481	0.0598

TABLE 1. Global properties of the initial, intermediate and optimal configurations

second was the development of GRYFX, which by using a gyrokinetic response for the zonal flows and advanced nonlinear closures was able to overcome the shortcomings of gyrofluid codes in the 1990s (Dimits *et al.* 2000) while still maintaining their huge speed advantage over gyrokinetic codes (typically a GRYFX run will be 20 times faster and 100 times less expensive than, for example, a Gs2 run; Mandell & Dorland (2014)).

It is only right to point out in this discussion that this study focuses solely on the plasma core, and not on the reactor components or the plasma edge. It should be noted that though edge transport barriers can be achieved in combination with negative triangularity (Pochelon *et al.* 2012), the evolution of the temperature at the edge of the domain, here held constant, would be strongly altered if the edge of the plasma was modelled in addition to the core, and thus the problem of optimizing the performance of the plasma as whole is distinct from optimizing that of the core, as is discussed further in (Pochelon *et al.* 2012). In fact it is likely that the edge confinement would degrade as the triangularity becomes negative, reducing the favourability of negative triangularity regimes (see e.g. Merle *et al.* (2017)). Thus further work is needed to understand how these results would be modified if the plasma edge was modelled self-

consistently with the core. In light of these limitations, it would be most desirable in the future to incorporate this methodology in a holistic model of the device (including checks on magneto-hydrodynamic stability); in particular it would be desirable to control the safety factor profile to maintain values greater than one in the core to avoid the sawtooth instability (the small increase in the safety factor required is not expected to significantly affect the results presented here). However, while ultimately all parts of a tokamak must be considered, by finding ways to improve core performance, the demands placed upon the reactor design and the requirement for high plasma confinement in the edge can be lessened.

Having demonstrated the first successful optimisation of (core) confinement using a nonlinear model of turbulence, there are several directions that are immediately attractive to follow. The first is to use this technique to find optimal configurations for JET ahead of its first run using an active (deuterium-tritium) fuel mix in twenty years (using parameters that match JET far more closely than in this study). The second is to consider, in a similar fashion, ways in which the performance of ITER, the new, global fusion experiment being constructed, can be improved. It would also be important to extend GRYFX to consider electromagnetic effects and kinetic electron physics, and to include the effects of rotation, which are not considered here. Other priorities would be to include additional transport channels: electron and ion heat and particles, momentum, impurity transport and so on. The complex interplay between these channels can be the crucial factor in achieving higher performance (see e.g. Highcock *et al.* (2011)), and robust operation, and is an ideal area to study with a nonlinear framework such as CoRFU. The eventual goal is to switch to using optimisation algorithms which parallelize easily and can search for global maxima, and run a vast parallel blue-skies search for a dramatically optimised fusion reactor.

5. Acknowledgements

The authors of this paper are indebted to A. Schekochihin, T. Fülöp, G. Hammett, J. Ball, J. Citrin, M. Landremann, I. Abel, F. van Wyk, F. Parra, C. Roach, S. Newton, I. Pusztai and J. Omotani for helpful discussions, ideas and support. This work has been carried out within the framework of the EUROfusion Consortium and has received funding from the Euratom research and training programme 2014–2018 under grant agreement No 633053. The views and opinions expressed herein do not necessarily reflect those of the European Commission. This work has also been supported by the Framework grant for Strategic Energy Research (Dnr. 2014–5392) from Vetenskapsrådet. NRM is supported by the U.S. Department of Energy via the DOE CSGF program, provided under grant DE-FG02-97ER25308. This work used the TACC Stampede supercomputer and the ARCHER UK National Supercomputing Service (<http://www.archer.ac.uk>).

Appendix A. Equations underlying the optimisation framework

The equations that govern the system are presented in (Abel *et al.* (2013)), which builds upon an already large body of work (significantly Frieman & Chen (1982); Sugama & Horton (1998)).

They follow a multi-scale approach, with a clear separation in time between the evolution of the safety factor (the twist of the magnetic field lines, which evolves on the resistive timescale; Abel & Cowley (2013)), the evolution of the pressure (which evolves on the confinement timescale), and the evolution of the turbulence (which occurs on the timescale of the linear micro-instabilities which drive it). The equations governing

all three are

$$\frac{\partial q}{\partial t} = \frac{c}{4\pi^2} \frac{\partial}{\partial \psi} V' \langle \mathbf{E} \cdot \mathbf{B} \rangle_\psi \quad (\text{A1})$$

$$\frac{3}{2} \frac{1}{V'} \frac{\partial}{\partial t} V' \langle n_s \rangle_\psi T_s + \frac{1}{V'} \frac{\partial}{\partial \psi} V' \langle Q_s \rangle_\psi = S_s \quad (\text{A2})$$

and

$$\begin{aligned} \frac{\partial h_s}{\partial t} + \left(v_{\parallel} \hat{\mathbf{b}} + \mathbf{V}_{D_s} + \frac{c}{B} \hat{\mathbf{b}} \times \nabla \langle \varphi \rangle_{\mathbf{R}} \right) \cdot \nabla h_s \\ = \langle C [h_s] \rangle_{\mathbf{R}} + \frac{Z_s e F_s}{T_s} \frac{\partial \langle \varphi \rangle_{\mathbf{R}}}{\partial t} - \frac{\partial F_s}{\partial \psi} \left(\hat{\mathbf{b}} \times \nabla \langle \varphi \rangle_{\mathbf{R}} \right) \cdot \nabla \psi, \end{aligned} \quad (\text{A3})$$

respectively. In these equations, q is the magnetic safety factor, ψ is the poloidal magnetic flux which is contained within a flux surface, V is the volume of the flux surface, $V' = dV/d\psi$ is the incremental volume element (loosely, the flux surface area), \mathbf{E} is the electric field and \mathbf{B} the magnetic field, and $\langle \rangle_\psi$ denotes an average over the flux surface. The index s labels the charged particle species (e.g. electron, deuterium ion, tritium ion etc.), T_s and n_s are the species temperature and density, Q_s is the flux of heat across a flux surface, and S_s is a volumetric heat source. The quantity h_s is the fluctuating (turbulent) part of the particle distribution function, v_{\parallel} is the velocity along the field line, $\hat{\mathbf{b}} = \mathbf{B}/|\mathbf{B}|$, \mathbf{V}_{D_s} represents the effect of the magnetic field inhomogeneities on particle motion, φ is the perturbed electric potential, C represents the effects of collisions between particles, $Z_s e$ is the species charge and F_s is the equilibrium (slowly varying) component of the species distribution function. The operator $\langle \rangle_{\mathbf{R}}$ denotes an average over gyrophase at fixed gyrocentre location \mathbf{R} . The turbulent component of the heat flux Q_s can be trivially obtained from the turbulent distribution function h_s

$$Q_s = \left\langle \int d^3 \mathbf{v} \frac{m_s v^2}{2} \left[\left(\frac{c}{B} \hat{\mathbf{b}} \times \nabla \langle \varphi \rangle_{\mathbf{R}} \right) \cdot \nabla \psi \right] \langle h_s \rangle_{\mathbf{r}} \right\rangle_{\psi, t} \quad (\text{A4})$$

where $\langle \rangle_{\mathbf{r}}$ denotes a gyroaverage at constant particle position. The (usually) subdominant neoclassical component of the heat flux is modelled using analytical approximations (Chang & Hinton 1982), as are radiative losses due to Bremsstrahlung (Glasstone & Lovberg 1960).

Since we are seeking a steady state solution, equation (A1) is not evolved during this study. Instead we prescribe a fixed profile of surface averaged toroidal current. This causes q to change with the pressure gradient, not on the resistive timescale, during the evolution towards steady state, but once steady state is reached q ceases to evolve and the solution is self-consistent. Using the prescribed profile of toroidal current, a prescribed outer flux surface and the pressure profile, the poloidal flux (and hence the shape of the magnetic flux surfaces) can be determined using the Grad-Shafranov equation:

$$\Delta^* \psi = -4\pi R^2 \sum_s n_s T_s \left\{ \frac{d \ln n_s}{d\psi} + \frac{d \ln T_s}{d\psi} \right\} - I(\psi) \frac{dI}{d\psi}, \quad (\text{A5})$$

where Δ^* is the Grad-Shafranov operator

$$\Delta^* \psi = \left(\frac{\partial^2}{\partial R^2} - \frac{1}{R} \frac{\partial}{\partial R} + \frac{\partial^2}{\partial Z^2} \right) \psi. \quad (\text{A6})$$

Note that when using the CHEASE code (Lütjens *et al.* (1996)) to solve the Grad-Shafranov equation, the usual function $I \partial I / d\psi$ can be replaced as an input by the surface averaged toroidal current density, which is what is specified in this study.

The equation for the pressure (A 2) is evolved by TRINITY (Barnes *et al.* (2010); TRINITY is also capable of evolving the density and rotation, which are kept fixed for this study). This equation determines how the evolution of the pressure is governed by the total flux of heat, given sources and the shape of the magnetic flux surfaces (that is, the solution of the Grad-Shafranov equation). Since the solution of the Grad-Shafranov equation itself varies on the same timescale as the pressure, the solution is periodically updated with the new pressure profile until steady-state is reached. The pressure equation can be evolved separately for each charged species; in this study, to reduce expense, it is solved for the deuterium ions. It is then assumed that collisional processes will rapidly equilibrate the temperatures of all species, and hence that the temperatures of the electrons and tritium ions is the same as that of the deuterium ions. A fixed pressure is set at the outer magnetic flux surface ($\rho = 1$); this is set to a pressure to be expected at the edge of the core, that is, at the top of an edge transport barrier.

The turbulent distribution function, from which can be calculated the turbulent fluxes, is determined by the gyrokinetic equation (A 3). This can be rigorously derived from first principles using assumptions which are valid in a fusion reactor. However, it remains too expensive to solve for the purposes of this study.

Instead, velocity space integrals are taken of this equation to create a hierarchy of fluid moments. In the early 1990s, a set of closures for this hierarchy were developed which accurately captured the linear response for drift waves, as well as finite Larmor radius effects (Beer & Hammett 1996; Dorland & Hammett 1993; Hammett & Perkins 1990). Unfortunately, while successful in many cases, these “gyrofluid” models were unable to capture correctly two key properties of the turbulence, namely, the excitation of large-scale zonal flows (Dimitis *et al.* 2000) and the phenomenon of perpendicular nonlinear phase mixing (Tatsuno *et al.* 2009). This resulted in the over-prediction of heat fluxes by gyrofluid models. However, in recent years a new hybrid gyrofluid/gyrokinetic code has been developed, GRYFX (see Appendices B–D), which overcomes these weaknesses, producing excellent agreement with codes that solve the gyrokinetic equation (Fig. 7) whilst still taking orders of magnitude less time. As is described in the main text, a principle advance has been the use of a gyrokinetic solver for the linear zonal flow response (Appendix D). This enables GRYFX to capture the characteristic “Dimitis shift” (Dimitis *et al.* 2000), where, for the parameters used in Fig. 7, the turbulent transport is suppressed to negligible levels in the range $4 \leq (1/T_i)dT_i/d\rho \lesssim 5$ even though the temperature gradient is above the linear stability threshold. This nonlinear upshift in the threshold has long been attributed to zonal flow dynamics, and our results are consistent with this theory. At large temperature gradients, the turbulence is stronger and the zonal flows are not as effective at suppressing the turbulence. In this regime, new closures that model the effects of nonlinear phase mixing (Appendix C) are the dominant effect in reducing the gyrofluid heat flux predictions to gyrokinetic levels. It is also important to note that recent theoretical and numerical work has showed that higher velocity space moments are energetically sub-dominant in the regimes of interest, producing renewed confidence that a closure with a sufficient number of moments can capture the important dynamics (Schekochihin *et al.* 2016; Parker *et al.* 2016). In addition since GRYFX includes the full quadratic nonlinearity (the fourth term on the left hand side of equation (A 3)), it is expected to capture important new phenomena such as subcritical turbulence.

When using GRYFX to calculate the turbulent fluxes within TRINITY, it is essential to use sufficient resolution to resolve the turbulent phenomena, to check for any pathologies, and to ensure that the turbulent calculation has reached convergence. There are many turbulent phenomena that can make this challenging, particularly near the threshold for

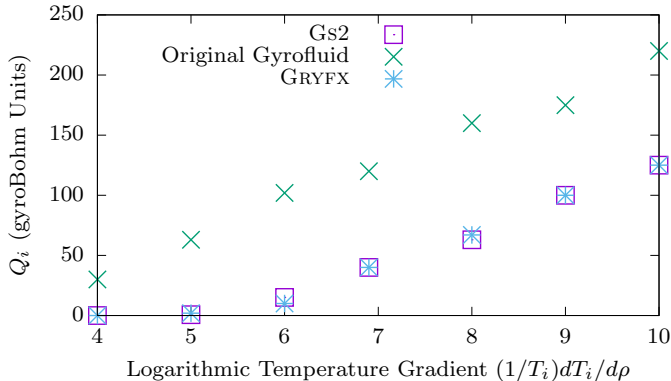


FIGURE 7. Comparison between gyrokinetic simulations (Gs2), the original gyrofluid model (Beer & Hammett (1996)), and GRYFX. The turbulent heat flux is shown as a function of the ion temperature gradient for Cyclone Base Case (Dimits *et al.* 2000) parameters.

the onset of turbulence, including long timescale oscillations and large amplitudes of the zonal flows. This is covered further in Appendix E.

Appendix B. Gyrofluid equations

The gyrofluid model in GRYFX is based on the 4+2 toroidal gyrofluid model of (Beer & Hammett 1996), which describes the time evolution of six guiding center moments of the gyrokinetic equation, (A 3): density (n), parallel velocity (u_{\parallel}), parallel and perpendicular temperature (T_{\parallel} and T_{\perp}), and the parallel fluxes of parallel and perpendicular heat (q_{\parallel} and q_{\perp}). These moments can be defined via the following velocity space integrals of the gyroaveraged fluctuating distribution function $g_s = h_s - (Z_s e/T_s) \langle \varphi \rangle_{\mathbf{R}} F_s$:

$$\begin{aligned}
 \delta n &= \int g \, d^3v & n_0 \delta u_{\parallel} &= \int g \, v_{\parallel} \, d^3v \\
 \delta p_{\parallel} &= T_s \delta n + n_s \delta T_{\parallel} = m_s \int g \, v_{\parallel}^2 \, d^3v & \delta p_{\perp} &= T_s \delta n + n_s \delta T_{\perp} = (m_s/2) \int g \, v_{\perp}^2 \, d^3v \\
 \delta q_{\parallel} &= -3n_s T_s \delta u_{\parallel} + m_s \int g \, v_{\parallel}^3 \, d^3v & \delta q_{\perp} &= -n_s T_s \delta u_{\parallel} + (m_s/2) \int g \, v_{\parallel} v_{\perp}^2 \, d^3v
 \end{aligned}$$

These fluctuating quantities (along with the electrostatic potential φ) are normalized as

$$\frac{a}{\rho_i} \left(\frac{\delta n}{n_s}, \frac{\delta u_{\parallel}}{v_{t,s}}, \frac{\delta T}{T_s}, \frac{\delta q}{n_s m_s v_{t,s}^3}, \frac{e\varphi}{T_i} \right) = \left(\tilde{n}, \tilde{u}_{\parallel}, \tilde{T}, \tilde{q}, \tilde{\varphi} \right) \quad (\text{B1})$$

where $v_{t,s} = \sqrt{T_s/m_s}$ is the ion thermal speed, n_s and T_s are the equilibrium ion density and temperature respectively, ρ_s is the ion gyroradius, and a is the normalizing length defined to be half the diameter of the last closed flux surface at the midplane. Here the subscript i denotes the reference ion species. These moment definitions follow (Snyder & Hammett 2001) and are consistent with Beer's original definitions. Note that we will evolve \tilde{T}_{\parallel} and \tilde{T}_{\perp} , whereas Beer used $\tilde{p}_{\parallel} = \tilde{n} + \tilde{T}_{\parallel}$ and $\tilde{p}_{\perp} = \tilde{n} + \tilde{T}_{\perp}$. Hereafter quantities will be normalised and non-dimensionalised unless otherwise specified, so we will drop the tildes unless they are necessary for clarity.† Further, note that these normalised moments are equivalent to the first several Laguerre-Hermite velocity moments of g , as described

† Our non-dimensionalisation is chosen to be consistent with Appendix A of (Mandell *et al.* 2018).

in (Mandell *et al.* 2018):

$$\left(G_{0,0}, G_{0,1}, \sqrt{2}G_{0,2}, \sqrt{6}G_{0,3}, G_{1,0}, G_{1,1}\right) = (n, u_{\parallel}, T_{\parallel}, q_{\parallel}, T_{\perp}, q_{\perp}), \quad (\text{B2})$$

where the Laguerre-Hermite moments are defined by (again in non-dimensional form)

$$G_{\ell,m} = 2\pi \int_{-\infty}^{\infty} dv_{\parallel} \int_0^{\infty} d\mu B \frac{(-1)^{\ell}}{\sqrt{m!}} L_{\ell}(\mu B) \text{He}_m(v_{\parallel}) g \quad (\text{B3})$$

with L_{ℓ} the Laguerre polynomials and He_m the probabilist's Hermite polynomials.

The gyrofluid equations that we solve in GRYFX can then be written as

$$\begin{aligned} \frac{\partial n}{\partial t} + \mathcal{N}_n + B\nabla_{\parallel} \frac{u_{\parallel}}{B} - \left(\frac{1}{L_{ns}} + \frac{1}{2L_{Ts}} \hat{\nabla}_{\perp}^2 \right) i\omega_{*}\Phi \\ + \left(2 + \frac{1}{2} \hat{\nabla}_{\perp}^2 \right) i\omega_d \Phi + i\omega_d (T_{\parallel} + T_{\perp} + 2n) = 0 \end{aligned} \quad (\text{B4})$$

$$\begin{aligned} \frac{\partial u_{\parallel}}{\partial t} + \mathcal{N}_{u_{\parallel}} + B\nabla_{\parallel} \frac{n + T_{\parallel}}{B} + \nabla_{\parallel} \Phi + \left(T_{\perp} + n + \frac{1}{2} \hat{\nabla}_{\perp}^2 \Phi \right) \nabla_{\parallel} \ln B \\ + i\omega_d (q_{\parallel} + q_{\perp} + 4u_{\parallel}) = 0 \end{aligned} \quad (\text{B5})$$

$$\begin{aligned} \frac{\partial T_{\parallel}}{\partial t} + \mathcal{N}_{T_{\parallel}} + B\nabla_{\parallel} \frac{q_{\parallel} + 2u_{\parallel}}{B} + 2(q_{\perp} + u_{\parallel}) \nabla_{\parallel} \ln B - \frac{1}{L_{Ts}} i\omega_{*}\Phi + 2i\omega_d \Phi \\ + i\omega_d (6T_{\parallel} + 2n) + 2|\omega_d| (\nu_1 T_{\parallel} + \nu_2 T_{\perp}) = -\frac{2}{3} \nu_{ss} (T_{\parallel} - T_{\perp}) \end{aligned} \quad (\text{B6})$$

$$\begin{aligned} \frac{\partial T_{\perp}}{\partial t} + \mathcal{N}_{T_{\perp}} - B\nabla_{\parallel} \frac{u_{\parallel}}{B} + B^2 \nabla_{\parallel} \frac{q_{\perp} + u_{\parallel}}{B^2} - \left[\frac{1}{2L_{ns}} \hat{\nabla}_{\perp}^2 + \frac{1}{L_{Ts}} \left(1 + \hat{\nabla}_{\perp}^2 \right) \right] i\omega_{*}\Phi \\ + \left(1 + \hat{\nabla}_{\perp}^2 + \hat{\nabla}_{\perp}^2 \right) i\omega_d \Phi + i\omega_d (4T_{\perp} + n) + 2|\omega_d| (\nu_3 T_{\parallel} + \nu_4 T_{\perp}) = \frac{1}{3} \nu_{ss} (T_{\parallel} - T_{\perp}) \end{aligned} \quad (\text{B7})$$

$$\begin{aligned} \frac{\partial q_{\parallel}}{\partial t} + \mathcal{N}_{q_{\parallel}} + (3 + \beta_{\parallel}) \nabla_{\parallel} T_{\parallel} + \sqrt{2} D_{\parallel} |k_{\parallel}| q_{\parallel} + i\omega_d (-3q_{\parallel} - 3q_{\perp} + 6u_{\parallel}) \\ + |\omega_d| (\nu_5 u_{\parallel} + \nu_6 q_{\parallel} + \nu_7 q_{\perp}) = -\nu_{ss} q_{\parallel} \end{aligned} \quad (\text{B8})$$

$$\begin{aligned} \frac{\partial q_{\perp}}{\partial t} + \mathcal{N}_{q_{\perp}} + \nabla_{\parallel} \left(T_{\perp} + \frac{1}{2} \hat{\nabla}_{\perp}^2 \Phi \right) + \sqrt{2} D_{\perp} |k_{\parallel}| q_{\perp} + \left(T_{\perp} - T_{\parallel} + \hat{\nabla}_{\perp}^2 \Phi - \frac{1}{2} \hat{\nabla}_{\perp}^2 \Phi \right) \nabla_{\parallel} \ln B \\ + i\omega_d (-q_{\parallel} - q_{\perp} + u_{\parallel}) + |\omega_d| (\nu_8 u_{\parallel} + \nu_9 q_{\parallel} + \nu_{10} q_{\perp}) = -\nu_{ss} q_{\perp} \end{aligned} \quad (\text{B9})$$

where

$$\begin{aligned} \nabla_{\parallel} &= v_{ts} \hat{\mathbf{b}} \cdot \nabla, & b &= k_{\perp}^2 \rho_s^2, & \Phi &= \Gamma_0^{1/2} (b) \varphi, & \mathbf{v}_{\Phi} &= \hat{\mathbf{b}} \times \nabla \Phi, \\ \frac{1}{2} \hat{\nabla}_{\perp}^2 \Phi &= b \frac{\partial \Gamma_0^{1/2}}{\partial b} \varphi, & \hat{\nabla}_{\perp}^2 \Phi &= b \frac{\partial^2}{\partial b^2} (b \Gamma_0^{1/2}) \varphi, \\ i\omega_{*} &= -\nabla \psi \cdot \hat{\mathbf{b}} \times \nabla, & i\omega_d &= \frac{\tau_s}{Z_s B^2} \hat{\mathbf{b}} \times \nabla B \cdot \nabla, \end{aligned}$$

and the species thermal velocity v_{ts} , gyroradius ρ_s , temperature τ_s , charge Z_s , equilibrium density and temperature scale lengths L_{ns} and L_{Ts} , and collision frequency ν_{ss} have all been non-dimensionalised. The nonlinear terms are denoted by \mathcal{N} and will be addressed in detail in Appendix C; the final form of these terms is given in (C10–C15). The quasineutrality constraint for a single ion species is

$$n_e = \frac{n}{1 + b/2} - \frac{bT_{\perp}}{2(1 + b/2)^2} + (\Gamma_0 - 1)\varphi, \quad (\text{B10})$$

where $\Gamma_n(b) = I_n(b)e^{-b}$ and $I_n(b) = i^{-n}J_n(ib)$ is the modified Bessel function. When electrons are assumed to be adiabatic, which is the case for all results in this paper, we have

$$n_e = \frac{T_i}{T_e}(\varphi - \langle \varphi \rangle_\psi), \quad (\text{B 11})$$

where $\langle \varphi \rangle_\psi$ is a flux surface average.

The coefficients D_\parallel , D_\perp , β_\parallel , and $\nu_1 - \nu_{10}$ are set by the closures and taken to be the same as in (Beer & Hammett 1996). These closure approximations are carefully chosen to capture important kinetic effects, notably Landau damping, phase mixing from toroidal ∇B and curvature drifts, and finite Larmor radius (FLR) effects. The resulting gyrofluid model can reproduce the gyrokinetic linear dispersion relation quite accurately.

Appendix C. Closures for nonlinear FLR phase mixing

Phase mixing processes, like Landau damping, are fundamentally caused by the fact that particles have a distribution of velocities. For the case of Landau damping, the spread in parallel velocities of particles freely streaming along field lines causes neighboring particles to move apart. This (linear) phase mixing process smears away spatial perturbations, even in the collisionless limit, and drives the formation of small-scale structures in $f(v_\parallel)$, with $\delta v_\parallel \sim 1/k_\parallel t$.

A similar phase mixing process is associated with the nonlinear term in the gyrokinetic equation. This term represents random mixing by gyro-averaged $\mathbf{E} \times \mathbf{B}$ flows, and thus produces small scale structure in space. There is a spread in the gyro-averaged $\mathbf{E} \times \mathbf{B}$ velocities of particles, as higher energy particles with larger gyroradii average over more fluctuations in the potential and thereby have a slower $\mathbf{E} \times \mathbf{B}$ drift than lower energy particles with smaller gyroradii. This leads to phase mixing perpendicular to the field and drives the formation of structure in $f(v_\perp)$. Thus the nonlinear term simultaneously produces small scale structures in both physical space and perpendicular velocity space.

This process was first recognized in the context of gyrofluid closures by Dorland & Hammett (1993). Later, Schekochihin *et al.* (2009) identified the existence of a kinetic cascade due to nonlinear phase mixing. They predicted the key properties of this cascade, and placed it in the context of the broader concept of entropy cascades. Notably, nonlinear phase mixing was found to be the dominant method of generating small-scale structure in velocity space, outpacing Landau damping. Tatsuno *et al.* (2012) studied nonlinear phase mixing in the context of freely decaying turbulence, identifying three regimes of importance, from collisional to collisionless. Howes *et al.* (2011) found numerical evidence supporting the existence of nonlinear phase mixing and the entropy cascade at small scales in electromagnetic, kinetic Alfvén wave turbulence. The effects of nonlinear phase mixing have also been observed experimentally, in laboratory magnetized plasmas (Kawamori 2013) and in the solar wind (Chen *et al.* 2010).

We will now derive a gyrofluid closure to model the effects of nonlinear FLR phase mixing. We start with a simple kinetic problem from which we derive a damped kinetic response. We then choose a dissipative gyrofluid closure and fit closure coefficients so that the gyrofluid response closely matches the kinetic response.

C.1. Simple kinetic problem

To illustrate the essence of the nonlinear phase mixing process, we follow Dorland & Hammett (1993) and start with a kinetic picture in sheared slab geometry. We consider a zonal potential that varies sinusoidally in only the x direction with wavenumber k_x :

$\varphi = \varphi_{ZF}(x) = \phi_{ZF} \sin(k_x x)$. The zonal $\mathbf{E} \times \mathbf{B}$ flow is then $\mathbf{v}_E = v_E(x) \hat{y} = \frac{\partial \varphi_{ZF}}{\partial x} \hat{y} = k_x \phi_{ZF} \cos(k_x x) \hat{y}$. Assuming no gradients in the equilibrium F_0 and no parallel gradients, the gyrokinetic equation reduces to a one-dimensional advection equation involving the nonlinear term,

$$\frac{\partial g}{\partial t} + J_0 \left(\frac{k_x v_\perp}{\Omega} \right) v_E \frac{\partial g}{\partial y} = 0. \quad (\text{C1})$$

Taking a Maxwellian initial perturbation with a single mode in y with wavenumber k_y , $g(t=0) = e^{ik_y y} F_M$, the perturbation then evolves as

$$g(t) = F_M e^{ik_y [y - J_0 (k_x v_\perp / \Omega) v_E t]} \simeq F_M e^{ik_y (y - v_E t)} e^{ik_y b v_E t v_\perp^2 / 4 v_i^2}, \quad (\text{C2})$$

where on the right we have expanded to first order in small b by taking $J_0 \simeq 1 - \frac{b}{4} v_\perp^2$, and here $b = k_x^2 v_i^2 / \Omega^2 = k_x^2 \rho^2$. In this small- $k_\perp \rho$ limit we can analytically calculate the kinetic perturbed density response, given by

$$n_{kin}(t) = \frac{1}{n_0} \int d^3 v g \simeq e^{ik_y (y - v_E t)} \frac{1}{1 - ik_y b v_E t / 2}. \quad (\text{C3})$$

Thus we see that the density response decays in time with a long tail that goes like $1/t$. This is the behavior that we will want to capture with our fluid closure. Note that we can also numerically integrate the exact kinetic solution in (C2) to capture the full J_0 effects; for $k_\perp \rho \leq 1$ the exact response is nearly identical to the small- $k_\perp \rho$ response given in (C3).

C.2. Fluid picture

If we take Laguerre moments in $\mu B = v_\perp^2 / 2$ of our simple 1D gyrokinetic equation (C1), we will see that each Laguerre moment is coupled via the nonlinear term, which is a manifestation of the phase mixing process (Mandell *et al.* 2018). Examining the equations for the first two Laguerre moments, $G_{0,0} = n$ and $G_{1,0} = T_\perp$, and again taking the small- $k_\perp \rho$ limit, we have

$$\frac{\partial n}{\partial t} + \left(1 - \frac{b}{2} \right) v_E \frac{\partial n}{\partial y} - \frac{b}{2} v_E \frac{\partial T_\perp}{\partial y} = 0, \quad (\text{C4})$$

$$\frac{\partial T_\perp}{\partial t} + \left(1 - \frac{3b}{2} \right) v_E \frac{\partial T_\perp}{\partial y} - \frac{b}{2} v_E \frac{\partial n}{\partial y} - \frac{b}{2} v_E \frac{\partial G_{2,0}}{\partial y} = 0, \quad (\text{C5})$$

where the $G_{2,0}$ Laguerre moment is not evolved but requires closure. These equations are identical to the Beer equations in the 1D low $k_\perp \rho$ limit, with the exception of the last $G_{2,0}$ term in (C5). Now that we have identified this extra term, we can generalize these equations to 3D, and to higher $k_\perp \rho$ using the full FLR expressions (Dorland & Hammett 1993):

$$\frac{\partial n}{\partial t} + \mathbf{v}_\Phi \cdot \nabla n + \left[\frac{1}{2} \hat{\nabla}_\perp^2 \mathbf{v}_\Phi \right] \cdot \nabla T_\perp = 0, \quad (\text{C6})$$

$$\frac{\partial T_\perp}{\partial t} + \mathbf{v}_\Phi \cdot \nabla T_\perp + \left[\frac{1}{2} \hat{\nabla}_\perp^2 \mathbf{v}_\Phi \right] \cdot \nabla n + \left[\hat{\nabla}_\perp^2 \mathbf{v}_\Phi \right] \cdot \nabla T_\perp + \left[\frac{1}{2} \hat{\nabla}_\perp^2 \mathbf{v}_\Phi \right] \cdot \nabla G_{2,0} = 0. \quad (\text{C7})$$

C.3. Fluid closure

Now we must find a closure expression for the extra term involving $G_{2,0}$ in (C7). If we simply set $G_{2,0} = 0$, as Beer did, we get an oscillatory (undamped) solution for n and T_\perp . In the spirit of the closures pioneered by Hammett and Perkins to model Landau

damping (Hammett & Perkins 1990), we can instead use dissipative closures to produce fluid density and temperature responses that are damped like the kinetic responses. Thus we will choose a closure of the form

$$G_{2,0} = \frac{\left[\frac{1}{2} \hat{\nabla}_{\perp}^2 \mathbf{v}_{\Phi} \right] \cdot \nabla}{\left[\frac{1}{2} \hat{\nabla}_{\perp}^2 \mathbf{v}_{\Phi} \right] \cdot \nabla} (\mu_1 n + \mu_2 T_{\perp}), \quad (\text{C } 8)$$

where we follow (Beer & Hammett 1996) and allow each coefficient μ to have a dissipative and a reactive (non-dissipative) piece, given by

$$\mu = \mu_r + \mu_i \frac{\left[\frac{1}{2} \hat{\nabla}_{\perp}^2 \mathbf{v}_{\Phi} \right] \cdot \nabla}{\left[\frac{1}{2} \hat{\nabla}_{\perp}^2 \mathbf{v}_{\Phi} \right] \cdot \nabla} = (\mu_r, \mu_i). \quad (\text{C } 9)$$

We set the μ_1 and μ_2 coefficients by numerically minimizing the difference between the kinetic density response (C 3) and the fluid density response found by evolving the n and T_{\perp} equations after inserting the closures. We have found that $\mu_1 = (0.747, -0.078)$ and $\mu_2 = (1.368, -2.023)$ produces a fluid response that fits the kinetic response reasonably well for $k_{\perp} \rho \lesssim 1$.

C.4. Extension to other moment equations

One can follow a similar procedure to develop nonlinear phase mixing closures for the remaining gyrofluid equations in the 4+2 model. The u_{\parallel} and q_{\perp} equations form a coupled system identical to the system we have studied above, so we can use the same 2-moment closure and simply replace n and T_{\perp} with u_{\parallel} and q_{\perp} , respectively. The T_{\parallel} and q_{\parallel} equations are also identical; each of these is not coupled to other equations, so the closures that appear in these equations are 1-moment closures. The closure coefficient is found with a similar procedure to the one used above, by fitting the fluid response for T_{\parallel} to the corresponding kinetic response.

This completes our derivation of a gyrofluid closure to model nonlinear FLR phase mixing. Adding these new terms to the original nonlinear terms, the final gyrofluid nonlinear terms used in GRYFX are given by

$$\mathcal{N}_n = \mathbf{v}_{\Phi} \cdot \nabla n + \left[\frac{1}{2} \hat{\nabla}_{\perp}^2 \mathbf{v}_{\Phi} \right] \cdot \nabla T_{\perp}, \quad (\text{C } 10)$$

$$\mathcal{N}_{u_{\parallel}} = \mathbf{v}_{\Phi} \cdot \nabla u_{\parallel} + \left[\frac{1}{2} \hat{\nabla}_{\perp}^2 \mathbf{v}_{\Phi} \right] \cdot \nabla q_{\perp}, \quad (\text{C } 11)$$

$$\mathcal{N}_{T_{\parallel}} = \mathbf{v}_{\Phi} \cdot \nabla T_{\parallel} + \left[\frac{1}{2} \hat{\nabla}_{\perp}^2 \mathbf{v}_{\Phi} \right] \cdot \nabla \left| \mu_3 T_{\parallel} \right|, \quad (\text{C } 12)$$

$$\mathcal{N}_{T_{\perp}} = \mathbf{v}_{\Phi} \cdot \nabla T_{\perp} + \left[\frac{1}{2} \hat{\nabla}_{\perp}^2 \mathbf{v}_{\Phi} \right] \cdot \nabla n + \left[\hat{\nabla}_{\perp}^2 \mathbf{v}_{\Phi} \right] \cdot \nabla T_{\perp} + \left[\frac{1}{2} \hat{\nabla}_{\perp}^2 \mathbf{v}_{\Phi} \right] \cdot \nabla \left| (\mu_1 n + \mu_2 T_{\perp}) \right|, \quad (\text{C } 13)$$

$$\mathcal{N}_{q_{\parallel}} = \mathbf{v}_{\Phi} \cdot \nabla q_{\parallel} + \left[\frac{1}{2} \hat{\nabla}_{\perp}^2 \mathbf{v}_{\Phi} \right] \cdot \nabla \left| \mu_3 q_{\parallel} \right|, \quad (\text{C } 14)$$

$$\mathcal{N}_{q_{\perp}} = \mathbf{v}_{\Phi} \cdot \nabla q_{\perp} + \left[\frac{1}{2} \hat{\nabla}_{\perp}^2 \mathbf{v}_{\Phi} \right] \cdot \nabla u_{\parallel} + \left[\hat{\nabla}_{\perp}^2 \mathbf{v}_{\Phi} \right] \cdot \nabla q_{\perp} + \left[\frac{1}{2} \hat{\nabla}_{\perp}^2 \mathbf{v}_{\Phi} \right] \cdot \nabla \left| (\mu_1 u_{\parallel} + \mu_2 q_{\perp}) \right|, \quad (\text{C } 15)$$

where \mathcal{N}_m represents the nonlinear terms in the m moment equation, and the absolute value terms comprise our new closure terms with closure coefficients

$\mu_1 = (0.747, -0.078)$, $\mu_2 = (1.368, -2.023)$, and $\mu_3 = (0.456, -0.724)$. This set of closures is similar to those presented in (Dorland & Hammett 1993), but that model required higher order terms of order $k_\perp^4 \rho^4$ in the n and u_\parallel equations, which is beyond the order of accuracy of the usual FLR terms. We avoid this by including closure terms proportional to n and u_\parallel in the T_\perp and q_\perp equations, respectively.

In the derivation of these new closures, we only considered nonlinear FLR phase mixing from a static, 1D potential. In an evolving 3D system, the phase mixing process is much more complicated, and our rough model may overestimate or underestimate the amount of phase mixing. Nonetheless, our model will capture the correct scaling of the mixing, producing physically motivated damping at large φ and high k_\perp . In this way our new terms can be interpreted as a type of hyperviscosity, but one that damps at the ρ scale as opposed to conventional hyperviscosity models that damp at the grid scale.

Finally we must address how we evaluate and implement a term of the form $\mathcal{P} = |\mathbf{v} \cdot \nabla| M$. Since we use a Fourier spectral representation for the equations, we are interested in the Fourier transform of \mathcal{P} . Denoting the Fourier transform of a quantity x as \hat{x}_k , and defining $\mathcal{N} = \mathbf{v} \cdot \nabla M$, we evaluate the closure term as

$$\hat{\mathcal{P}}_k = (|\widehat{\mathbf{v} \cdot \nabla} M)_k = |\hat{\mathcal{N}}_k| \frac{\hat{M}_k}{|\hat{M}_k|}, \quad (\text{C } 16)$$

where all operations are performed in Fourier space, and $\hat{\mathcal{N}}_k$ can be calculated pseudospectrally in the same manner as the usual nonlinear terms.

Appendix D. Hybrid gyrokinetic-gyrofluid zonal flow model

A major drawback of the Beer gyrofluid model is the inability to accurately model zonal flows. These nonlinearly-driven sheared poloidal $\mathbf{E} \times \mathbf{B}$ flows have been shown to play a key role in determining the turbulence saturation level. Therefore inaccuracy in zonal flow dynamics has been one of the main sources of disagreement between gyrofluid and gyrokinetic turbulence models.† Attempts were made, with limited success, to modify the gyrofluid closures (Beer & Hammett 1998) to capture the linearly undamped component of the flows derived by Rosenbluth & Hinton (1998). These closure modifications had limited success (Dimitis *et al.* 2000), and also relied on simplifying assumptions about the magnetic geometry, which would not be able to capture the dependence of zonal flow dynamics on shaping (Xiao *et al.* 2007). Further, accurately modeling zonal flows involves resolving sharp features in the distribution function in the v_\parallel direction resulting from trapped particle dynamics, which in a moment approach would require much higher Hermite moments in v_\parallel than used in the Beer model (Mandell *et al.* 2018).

Instead of seeking more complicated gyrofluid closure modifications to improve zonal flow accuracy, we avoid this issue by employing a hybrid approach in GRYFX: we evolve the zonal flow modes with a fully gyrokinetic model (using the gyrokinetic code Gs2), while continuing to evolve the non-zonal modes with the gyrofluid model given by equations (B 4–B 9) above. Because we use a Fourier spectral representation for the perpendicular configuration space discretization in GRYFX, and because the Fourier modes only interact via the nonlinearity, we can easily choose an alternative algorithm for the linear evolution of the zonal ($k_y = 0$) modes. In order to nonlinearly couple

† This is not to say that zonal flow dynamics is the only source of disagreement. Our results indicate that even with accurate zonal flow dynamics, a model of nonlinear phase mixing is required to produce the agreement between the gyrofluid and gyrokinetic models shown in Figure 7.

the zonal and non-zonal modes, we must first be able to transform the gyrokinetic distribution function into gyrofluid moments, and vice versa. The transformation from the gyrokinetic distribution function to gyrofluid moments is simply the process of taking velocity moments, which can also be interpreted as projecting the distribution function onto a Laguerre-Hermite basis as shown in equation (B 3). For the inverse transformation, from gyrofluid moments to the gyrokinetic distribution function, we can expand the distribution function in the Laguerre-Hermite basis as (Mandell *et al.* 2018)

$$\frac{g}{F_0} = \sum_{\ell=0} \sum_{m=0} \frac{(-1)^\ell}{\sqrt{m!}} L_\ell(\mu B) \text{He}_m(v_{\parallel}) G_{\ell,m} \quad (\text{D } 1)$$

$$\begin{aligned} &\approx n + v_{\parallel} u_{\parallel} + \frac{1}{2} (v_{\parallel}^2 - 1) T_{\parallel} + (\mu B - 1) T_{\perp} \\ &\quad + \frac{1}{2} \left(\frac{v_{\parallel}^3}{3} - v_{\parallel} \right) q_{\parallel} + v_{\parallel} (\mu B - 1) q_{\perp} \end{aligned} \quad (\text{D } 2)$$

where in the second line we have explicitly expressed the expansion in terms of the Beer gyrofluid moments and truncated.

Following the same logic, we can expand the gyrokinetic nonlinear term in terms of the gyrofluid nonlinear terms given in (C 10–C 15):

$$\begin{aligned} \mathcal{N}_{gk} &= \hat{\mathbf{b}} \times \nabla \langle \varphi \rangle_{\mathbf{R}} \cdot \nabla h = \hat{\mathbf{b}} \times \nabla \langle \varphi \rangle_{\mathbf{R}} \cdot \nabla g \\ &\approx \mathcal{N}_n + v_{\parallel} \mathcal{N}_{u_{\parallel}} + \frac{1}{2} (v_{\parallel}^2 - 1) \mathcal{N}_{T_{\parallel}} + (\mu B - 1) \mathcal{N}_{T_{\perp}} \\ &\quad + \frac{1}{2} \left(\frac{v_{\parallel}^3}{3} - v_{\parallel} \right) \mathcal{N}_{q_{\parallel}} + v_{\parallel} (\mu B - 1) \mathcal{N}_{q_{\perp}}, \end{aligned} \quad (\text{D } 3)$$

Thus we can construct the gyrokinetic nonlinear term for the $k_y = 0$ zonal modes from the $k_y = 0$ component of the six gyrofluid nonlinear terms. The full hybrid algorithm then proceeds as follows.

(i) Calculate moments of the $k_y = 0$ component of the gyrokinetic distribution function (*e.g.* via (B 3)).

(ii) Evaluate the six gyrofluid nonlinear terms, (C 10–C 15), for all Fourier modes.

(iii) Evaluate the $k_y = 0$ component of the gyrokinetic nonlinear term via (D 3).

(iv) Evolve the $k_y \neq 0$ modes with equations (B 4–B 9).

(v) Evolve the $k_y = 0$ modes with equation (A 3) using the nonlinear term from (iii).

As mentioned above, we couple to the gyrokinetic code Gs2 to evolve the gyrokinetic equation in step (v). Further, we do not include the nonlinear phase mixing closure terms in the $k_y = 0$ component of the gyrofluid nonlinear terms. This is in part due to the fact that introducing damping from closure models can suppress the zonal flow residual (which is precisely the reason we moved to gyrokinetic evolution of the zonal modes). Thus in our model, the nonlinear drive for the zonal flows comes only from the lowest several moments of the distribution function; this approximation is justified by the results of (Rogers *et al.* 2000).

Finally, note that steps (iv) and (v) can be executed in parallel. In GRYFX we take advantage of GPU-CPU concurrency by simultaneously evolving the non-zonal gyrofluid equations on the GPU and the zonal gyrokinetic equation on the CPU. Using a single GPU and ~ 16 CPU cores (a common supercomputer node configuration), the two steps take roughly the same amount of wall clock time. This means that in our scheme the

additional cost (in terms of wall clock time) of using a fully gyrokinetic model for the zonal flows is minimal.

Appendix E. Practical Considerations

The presentation of equations and the methodology given above has, for reasons of clarity and brevity, skipped over some of the most thorny issues encountered during the current study. However, we believe that a discussion of them should be present in this work, and we hope that by including it here as an appendix, we can save at least some time and effort for future researchers. In this discussion it helps to think of the operation of CORFU as a series of six nested loops, as illustrated in Fig. 8. Within each of these loops issues can arise. The principle practical challenges encountered in the construction and use of the CORFU framework (independent of the challenges in constructing its individual components such as TRINITY or GRYFX) were:

- (i) incorporating evolution of the magnetic equilibrium,
- (ii) determining whether a particular turbulence calculation had reached steady state,
- (iii) encountering failures of either the turbulence code or the Grad-Shafranov (GS) code,
- (iv) dealing with turbulent thresholds,
- (v) making efficient use of resources, and
- (vi) choosing resolution parameters for the turbulence code.

In the following sections we discuss each of these challenges.

E.1. Incorporating evolution of the magnetic equilibrium

The TRINITY transport solver has the ability to evolve the magnetic equilibrium internally. However, at present it is not able to treat the evolution of the magnetic equilibrium implicitly, as it does the profiles of density, temperature and flow. Therefore it would be necessary to use a much smaller transport step to avoid numerical instability.

The advantage of this study is that we are only seeking steady-state transport and magnetic equilibrium solutions. Thus, provided TRINITY discovers a solution in which both the profiles and the equilibrium do not vary in time, this solution will be self-consistent and thus acceptable. This allows us to separate the evolution of the Grad-Shafranov solution from TRINITY, as is illustrated in Fig. 8. In effect, TRINITY evolves using a fixed magnetic equilibrium until the profiles stop changing. At this point the new pressure profile is passed to CHEASE which recalculates the equilibrium. TRINITY is then re-run with new equilibrium and the cycle is repeated until the optimisation criterion converges to within a specified tolerance (see Appendix E.2).

E.2. Determining whether a particular turbulence calculation had reached steady state

This is an extensive subject fraught with complication. Not only is it hard to automate what enters into human judgement in these cases (in many cases the best way of determining whether a simulation has reached saturation is to “eyeball” the time traces) but there are cases when even the best of classification systems would fail (e.g. the case of slow zonal flow amplitude rise in ETG turbulence; Colyer *et al.* (2017)).

The difficulty proceeds from having no *a priori* knowledge of the timescales of a given situation: in particular, those of the linear growth, time to saturation, and the longest timescales in the saturated state (usually related to zonal flows). A typical dilemma might be: is the heat flux no longer changing because

- (i) the simulation has reached a saturated nonlinear state, or

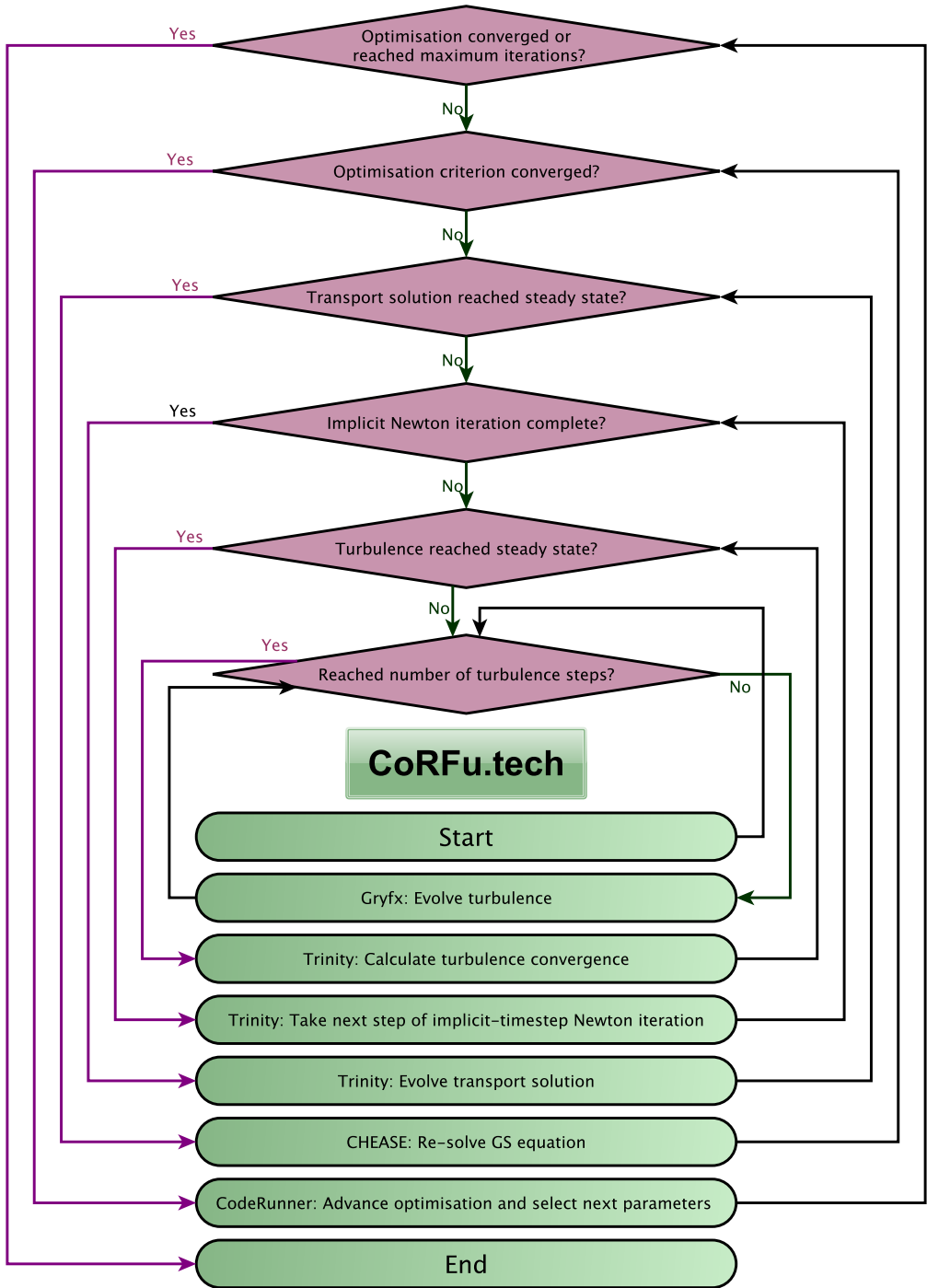


FIGURE 8. Schematic of CoRFU operation showing the hierarchy of decision loops which must be walked through.

- (ii) the system was stable and all modes died away to a constant noise level, or
- (iii) the growth rate was so small that the change in amplitude was undetectable on the timescale allotted?

The authors of this paper have experimented with many techniques, including rolling time averages, moving averages and frequency analysis. In this work, a simpler approach was used which represented a balance between the competing objectives of certainty, efficiency, and robustness.

Each turbulence calculation (that is, for each radial location, each element of the Jacobian and each transport iteration) was broken up into a number of stages, with all fields cached between stages so that the calculation could resume instantly from the same state. The number of time steps in each stage was chosen in combination with the timestep so that each stage lasted $O(10)$ turnover times (a/v_{thi}). The turbulence code driver then ran the calculation for two initial stages, and then proceeded to run each calculation according to the decision tree presented in Fig. 9. This decision tree is extremely restrictive about allowing a simulation to be declared converged. This choice was motivated by the observation that a bad value for the heat flux incurred such a great time penalty—by disrupting the sensitive implicit Newton iteration—that running GRYFX for a little longer than was typically necessary saved time in the long run.

E.3. Encountering failures of either Newton iteration, the turbulence code or the GS solver

It is of course possible for any component of CORFU to experience a failure during the very long operation typically required. This could be due to hardware failures, file corruptions, and so on. However, the three most common failures that were encountered were

- failure of the Newton iteration to converge due to overlarge timestep or a bad flux value,
- numerical instability from an overly large timestep in GRYFX, and
- failure of CHEASE to converge on a solution, usually as a result of a non-monotonic pressure profile but sometimes from straying to an extreme location in parameter space.

In the case of a failure of the Newton iteration, one likely cause was the inherent noise in the turbulent fluxes. In particular, this was a problem if a large change in a gradient (e.g. the temperature gradient $\kappa_T = R/L_T$) produced only a small change in a transport coefficient (e.g. the heat flux Q). Since we are inverting a Jacobian which essentially depends on quantities such as $\Delta Q/\Delta\kappa_T$, if the true value of ΔQ is small, and there is noise, of the same magnitude, which contrives to give ΔQ close to zero, there is an artificial stationary point created in the search domain which will lead the Newton iteration to take a large jump incorrectly. In the future, it is planned to implement a Levenberg-Marquardt mixed search which will be more resistant to this; for the current study it was necessary to be very stringent with the turbulence convergence conditions, and to use a large, fixed value of $\Delta\kappa_T = 0.6$. The reasoning behind this was that since $Q \propto \kappa_T^3$ (Barnes *et al.* 2011b), a constant value of $\Delta\kappa_T$ would continue to produce a respectable ΔQ as Q tended to 0, but would not produce an excessively large ΔQ far from the threshold.

With this implemented, a remaining likely cause of a failure was a real stationary point in the search domain, and the solution was to make the transport timestep smaller. In the next section we will discuss this in more detail with regard to efficiency. However, there was another consideration when resetting the timestep: what to do about the state of the turbulence calculation.

If the Newton iteration had deviated very far from the previous profiles it might be

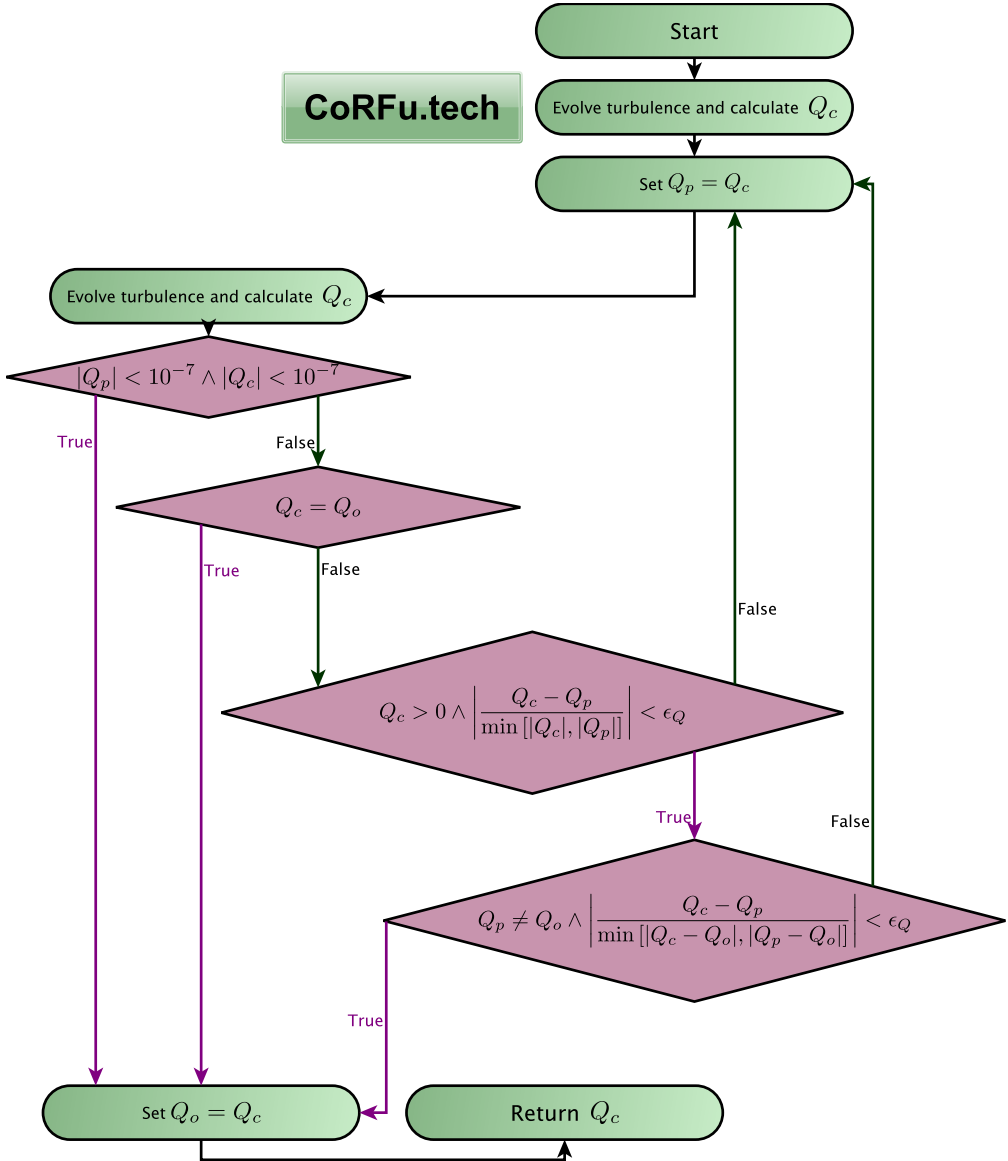


FIGURE 9. Schematic of the CoRFu turbulence code driver showing the logic used to determine if a turbulence calculation is saturated (Q_o is the heat flux from the previous iteration, Q_p is the heat flux from the previous stage of the turbulence calculation, and Q_c is the heat flux from the current stage).

reasonable to assume that since the turbulent state at the end of the failed iteration was very far from that at the beginning, it would be better to start the turbulence calculation from noise to avoid the turbulence displaying violent transients (particularly if the end of the failed iteration was in a strongly-driven regime). In fact, since (because of stiff transport) the steady-state profiles were never very far from marginal (with low growth rates), such a strategy would incur a large time penalty and run the risk of mistaking a low-growing turbulent case for a stable case.

In the case of GRYFX, a timestep was chosen that was sufficiently small for almost

all cases. The turbulence calculation driver would typically start a GRYFX simulation stage using the state of the previous simulation stage (since either it was continuing a calculation till convergence, or it was starting a new calculation with similar parameters to the previous); however this behaviour was changed if necessary (note that resetting the initial condition close to threshold when the growth rate was low incurred a significant time penalty). Otherwise, the following steps were taken to mitigate problems:

- If the previous TRINITY Newton iteration did not converge, values of fields and moments were kept but time averages of fluxes were reset.
- If the previous fluxes were very small ($< 10^{-7}$), all values were reset.
- If the previous fluxes were either very large ($> 1e10$) or had NaN values, all values were reset. Typically this was because a quirk of the initial condition pushed the turbulence amplitudes to values too large for the timestep and could be fixed by resetting, but if this occurred repeatedly the optimisation would be halted and require intervention.
- If fewer than 3 turbulence stages had been run the moving averages would be reset to eliminate initial transients.
- If greater than 3 turbulence stages had been run, the timescale of the moving average would gradually increase in successive stages (proportional to the total turbulence time elapsed in these successive stages) to force eventual convergence of the heat flux. This was a necessary to ensure that the transport calculation never became stuck, and had no impact on the results, once again because only steady-state solutions were required.

In the case of the Grad-Shafranov solver CHEASE, since failures were often caused by an unconverged pressure profile, CoRFU first attempted to run TRINITY for an extra period of time using the previous equilibrium. Occasionally in preliminary studies (though not in the study reported here) the GS solver failed because the control parameters strayed into a region of parameter space where a solution could not be found. In such cases a highly unfavourable value was returned to prevent the algorithm pursuing that search direction.

E.4. Dealing with turbulent thresholds

To a user of the CoRFU framework, it is an inconvenient reality that optimal solutions typically lie close to the zero-turbulence manifold. This means that the transport solver TRINITY will spend most of its operation hovering around the turbulent threshold. This is a problem because of the extra time required to calculate the turbulent transport. If the previous transport iteration was below the threshold and the subsequent iteration is likewise, the turbulence calculation will end rapidly because any initial noise will die away. If the previous iteration was above threshold, and the subsequent one is too, then the turbulence will rapidly adjust to the new drive parameters. However, if the previous iteration was below threshold and the subsequent one above, (i.e the transport solver crosses the zero-turbulence manifold from below) the turbulence calculation will not converge until amplitudes have grown linearly to saturation amplitudes. Since we are close to threshold with small growth rates, this may take a very long time. Equally unpleasant is when the zero-turbulence manifold is crossed from above: in this case the free energy of the previous vigorous turbulence must be absorbed by only weakly damped modes.

The strategy for dealing with the zero-turbulence manifold was to adjust the way that TRINITY calculated the derivatives of fluxes (e.g. Q) with respect to profile gradients (e.g. κ_T). Effectively we needed to make sure that, as far as possible, the lower part of the derivative stencil stays below the threshold, and the higher part stays above the threshold. This is achieved firstly by ensuring that the stencil is always fairly broad (at the cost of reducing the convergence rate of the Newton iteration and hence the size of the timestep).

Fortunately, this requirement coincided with the requirement described in Appendix E.3 for a large ΔQ . The second way to achieve this is to set a tight convergence criterion for the Newton iteration to make sure that it rarely artificially (that is, at odds with the continuous time-evolution) crossed the threshold (in terms of TRINITY parameters, `errflr` was set to 0.02 and `flrfac` was set to 4.0).

E.5. *Making efficient use of resources*

Although GRYFX is a very fast and efficient code, it is very important, given the number of turbulence calculations carried out, to strictly control the cost of the optimisation study. For many reasons, as given above, it is necessary to be overly cautious and run the turbulence simulations until a strict set of criteria have been satisfied. Nonetheless, it will always be the case that during every iteration of the transport calculation some flux calculations will converge before others. Therefore the flux driver is set up so that the optimisation can run on an arbitrary number of GPUs, and that if the number of GPUs is less than the number of flux calculations carried out at a time, then at each stage of the flux calculation the GPUs will cycle through each of the flux calculations requested by the driver. As the number of stages increases, more and more of the turbulence calculations will have converged and so the GPUs will cycle more quickly through the remaining ones. In the current study, with eight flux calculations per transport iteration, running on four GPUs, this arrangement reduced the simulation cost by close to 50%.

An equally important consideration with regard to cost is the choices made for iteration and time stepping parameters within TRINITY. When seeking a steady state solution, a certain amount of time will need to elapse while the profiles adjust to the new parameters provided by the optimisation driver. A first assumption might be that increasing the size of the timestep will reduce the cost of evolving the profiles for that time (remembering that the TRINITY algorithm is implicit and therefore stable for large timesteps). However, the larger the timestep, the greater the difference between the profiles at the end and the profiles at the beginning of the timestep, and thus the greater the chance that the Newton search will not be able to land upon the future profiles. If this occurs, the timestep must be reduced and the step repeated, effectively doubling the cost of that timestep. Increasing the maximum number of steps in the Newton iteration would increase the chances of it reaching a solution; however, it would also increase the cost should the iteration still fail.

By trial and error, the following choices were found to enable efficient and robust operation.

- The threshold for rejecting a Newton iteration was set high (`errtol=0.1`) to avoid the cost of repeating an iteration (this value was still low enough to avoid wacky iterations triggered by a stationary point).
- The threshold for saying that the Newton iteration was converged and therefore fewer than the allowed number of steps were needed was set low (`errflr=0.02`) so that the iteration was always as accurate as possible, leading to an accurate time evolution.
- The threshold for increasing the timestep was set very low (`flrfac=4` so that the threshold was 0.02/4) so that the timestep was only increased if the iterations were proceeding very smoothly.
- The factor by which the timestep was reduced after a failed iteration was set high (`deltadj=4`) to avoid repeated failed iterations. For example, when crossing a turbulent threshold it was often necessary to rapidly reduce the transport timestep: if `deltadj` was small, it would take a long time before the timestep was reduced sufficiently.
- The maximum allowed number of steps in the Newton iteration was set to 4. This

represented a balance between giving the search the greatest chance of succeeding and reducing the cost if the search eventually failed.

E.6. Choosing resolution parameters for the turbulence code

The resolution required for the turbulence calculation, including perpendicular box size, perpendicular and parallel resolutions, and timestep, vary significantly with the values of the driving parameters and the magnetic geometry.

In the present case, the GPUs that were available for the calculation were sufficiently powerful to allow the increase of the GRVFX resolution to a size that was more than adequate for the majority of simulations (as determined by manual inspection of a sample of turbulence simulations), without an unmanageable increase in cost.

There are *a posteriori* ways of checking that resolutions were sufficient, such as examining turbulent spectra, which would allow one to avoid such a blanket cost increase. It is also, of course, possible to check that the output quantities such as heat flux do not change with increased resolution. However, the automation of such investigations, which are usually carried out by hand for individual turbulence calculations, has not yet been implemented in the CoRFU framework, and would constitute significant additional research.

REFERENCES

- ABEL, I. G. & COWLEY, S. C. 2013 Multiscale gyrokinetics for rotating tokamak plasmas: II. Reduced models for electron dynamics. *New Journal of Physics* **15**, arXiv: 1210.1417.
- ABEL, I. G., PLUNK, G. G., WANG, E., BARNES, M., COWLEY, S. C., DORLAND, W. & SCHEKOCHIHIN, A. A. 2013 Multiscale gyrokinetics for rotating tokamak plasmas: fluctuations, transport and energy flows. *Reports on progress in physics. Physical Society (Great Britain)* **76** (11), 116201.
- ABRAMSON, D., PEACHEY, T. & LEWIS, A. 2006 Model Optimization and Parameter Estimation with Nimrod / O. *Proceedings of the 6th international conference on Computational Science (ICCS'06)* **1**, 720–727.
- BARNES, M., ABEL, I. G., DORLAND, W., GORLER, T., HAMMETT, G. W. & JENKO, F. 2010 Direct multiscale coupling of a transport code to gyrokinetic turbulence codes. *Physics of Plasmas* **17** (5), 056109, arXiv: 0901.2868.
- BARNES, M., PARRA, F. I., HIGHCOCK, E. G., SCHEKOCHIHIN, A., COWLEY, S. C. & ROACH, C. M. 2011a Turbulent Transport in Tokamak Plasmas with Rotational Shear. *Physical Review Letters* **106** (17), 1–4.
- BARNES, M., PARRA, F. I. & SCHEKOCHIHIN, A. A. 2011b Critically Balanced Ion Temperature Gradient Turbulence in Fusion Plasmas. *Physical Review Letters* **107** (11), 115003.
- BEER, M. & HAMMETT, G. 1998 The dynamics of small-scale turbulence-driven flows. *Varenna Proceedings* pp. 1–11.
- BEER, M. A., COWLEY, S. C. & HAMMETT, G. W. 1995 Fieldaligned coordinates for nonlinear simulations of tokamak turbulence. *Physics of Plasmas* **2** (7), 2687–2700.
- BEER, M. A. & HAMMETT, G. W. 1996 Toroidal gyrofluid equations for simulations of tokamak turbulence. *Physics of Plasmas* **3** (11), 4046.
- BOURDELLE, C., CITRIN, J., BAIOCCHI, B., CASATI, A., COTTIER, P., GARBET, X. & IMBEAUX, F. 2016 Core turbulent transport in tokamak plasmas: bridging theory and experiment with QuaLiKiz. *Plasma Physics and Controlled Fusion* **58** (1), 014036.
- BUDNY, R. V. 2009 Comparisons of predicted plasma performance in ITER H-mode plasmas with various mixes of external heating. *Nuclear Fusion* **49** (8), 85008.
- BURRELL, K. H. 1997 Effects of ExB velocity shear and magnetic shear on turbulence and transport in magnetic confinement devices. *Physics of Plasmas* **4** (5), 1499–1518.
- CHANG, C. S. & HINTON, F. L. 1982 Effect of impurity particles on the finite-aspect ratio neoclassical ion thermal conductivity in a tokamak. *Physics of Fluids* **25** (1493), 3314.

- CHEN, C., WICKS, R., HORBURY, T. & SCHEKOCIHIN, A. 2010 Interpreting power anisotropy measurements in plasma turbulence. *The Astrophysical Journal Letters* **711** (2), L79.
- CITRIN, J., BRETON, S., FELICI, F., IMBEAUX, F., ANIEL, T., ARTAUD, J. F., BAIOCCHI, B., BOURDELLE, C., CAMENEN, Y. & GARCIA, J. 2015a Real-time capable first principle based modelling of tokamak turbulent transport. *Nuclear Fusion* **55** (9), 92001, arXiv: 1502.07402v1.
- CITRIN, J., GARCIA, J., GÖRLER, T., JENKO, F., MANTICA, P., TOLD, D., BOURDELLE, C., HATCH, D. R., HOGEWELJ, G. M. D., JOHNSON, T., PUESCHEL, M. J. & SCHNEIDER, M. 2015b Electromagnetic stabilization of tokamak microturbulence in a high- β regime. *Plasma Physics and Controlled Fusion* **57** (1), 014032.
- CITRIN, J., JENKO, F., MANTICA, P., TOLD, D., BOURDELLE, C., DUMONT, R., GARCIA, J., HAVERKORT, J., HOGEWELJ, G., JOHNSON, T. & PUESCHEL, M. 2014 Ion temperature profile stiffness: non-linear gyrokinetic simulations and comparison with experiment. *Nuclear Fusion* **54** (2), 023008.
- COLYER, G. J., SCHEKOCIHIN, A. A., PARRA, F. I., ROACH, C. M., BARNES, M. A., GHIM, Y. C. & DORLAND, W. 2017 Collisionality scaling of the electron heat flux in ETG turbulence. *Plasma Physics and Controlled Fusion* **59** (5), arXiv: 1607.06752.
- DIMITS, A. M., BATEMAN, G., BEER, M. A., COHEN, B. I., DORLAND, W., HAMMETT, G. W., KIM, C., KINSEY, J. E., KOTSCHENREUTHER, M., KRITZ, A. H., LAO, L. L., MANDREKAS, J., NEVINS, W. M., PARKER, S. E., REDD, A. J., SHUMAKER, D. E., SYDORA, R. & WEILAND, J. 2000 Comparisons and physics basis of tokamak transport models and turbulence simulations. *Physics of Plasmas* **7** (3), 969.
- DORLAND, W. & HAMMETT, G. W. 1993 Gyrofluid Turbulence Models with Kinetic Effects. *Physics of Fluids B-Plasma Physics* **5**, 812–835.
- DORLAND, W., JENKO, F., KOTSCHENREUTHER, M. & ROGERS, B. N. 2000 Electron temperature gradient turbulence. *Physical review letters* **85** (26 Pt 1), 5579–5582.
- EJ DOYLE, WA HOULBERG, KAMADA, Y., V MUKHOVATOV, TH OSBORNE, A POLEVOI, BATEMAN, G., JW CONNOR, JG CORDEY, T FUJITA, X GARBET, TS HAHM, LD HORTON, AE HUBBARD, F IMBEAUX, F JENKO, J. E. KINSEY, Y KISHIMOTO, J LI, TC LUCE, Y MARTIN, M OSSIPENKO, V PARAIL, A PEETERS, TL RHODES, JE RICE, ROACH, C. M., ROZHANSKY, V., RYTER, F., G SAIBENE, R SARTORI, ACC SIPS, JA SNIPES, M SUGIHARA, EJ SYNAKOWSKI, H TAKENAGA, T TAKIZUKA, K THOMSEN, MR WADE, HR WILSON, ITPA TRANSPORT PHYSICS TOPICAL GROUP, ITPA CONFINEMENT DATABASE, MODELLING TOPICAL GROUP, ITPA PEDESTAL, EDGE TOPICAL GROUP, PHYSICS), E. J. D. C. T., DATABASE, W. A. H. C. C., PEDESTAL, Y. K. C., PHYSICS), V. M. C.-C. T., PEDESTAL, T. H. O. C.-C., DATABASE, A. P. C.-C. C., BATEMAN, G., CONNOR, J. W., (RETIRED), J. G. C., FUJITA, T., GARBET, X., HAHM, T. S., HORTON, L. D., HUBBARD, A. E., IMBEAUX, F., JENKO, F., KINSEY, J. E., KISHIMOTO, Y., LI, J., LUCE, T. C., MARTIN, Y., OSSIPENKO, M., PARAIL, V., PEETERS, A., RHODES, T. L., RICE, J. E., ROACH, C. M., ROZHANSKY, V., RYTER, F., SAIBENE, G., SARTORI, R., SIPS, A. C. C., SNIPES, J. A., SUGIHARA, M., SYNAKOWSKI, E. J., TAKENAGA, H., TAKIZUKA, T., THOMSEN, K., WADE, M. R., WILSON, H. R., GROUP, I. T. P. T., DATABASE, I. C., GROUP, M. T., PEDESTAL, I., GROUP, E. T., DOYLE, E. J., HOULBERG, W. A., KAMADA, Y., MUKHOVATOV, V., OSBORNE, T. H., POLEVOI, A. & CORDEY, J. G. 2007 Chapter 2: Plasma confinement and transport. *Nuclear Fusion* **47** (6), S18.
- ESTECO, M. 2018 modeFrontier Home Page. <http://www.esteco.com/modefrontier>.
- FEDERICI, G., KEMP, R., WARD, D., BACHMANN, C., FRANKE, T., GONZALEZ, S., LOWRY, C., GADOMSKA, M., HARMAN, J., MESZAROS, B., MORLOCK, C., ROMANELLI, F. & WENNINGER, R. 2014 Overview of EU DEMO design and R&D activities. *Fusion Engineering and Design* **89** (7-8), 882–889.
- FRIEMAN, E. A. & CHEN, L. 1982 Nonlinear gyrokinetic equations for low-frequency electromagnetic waves in general plasma equilibria. *Physics of Fluids* **25** (3), 502.
- GALAMBOS, J., PERKINS, L., HANEY, S. & MANDREKAS, J. 1995 Commercial tokamak reactor potential with advanced tokamak operation. *Nuclear Fusion* **35** (5), 551–573.
- GLASSTONE, S. & LOVBERG, R. H. 1960 Controlled Thermonuclear Reactions. D. Van Nostrand Company.
- HAMMETT, G. W. & PERKINS, F. W. 1990 Fluid moment models for Landau damping with

- application to the ion-temperature-gradient instability. *Physical review letters* **64** (25), 3019–3022.
- HIGHCOCK, E. G., BARNES, M., PARRA, F. I., SCHEKOCIHIN, A. A., ROACH, C. M. & COWLEY, S. C. 2011 Transport bifurcation induced by sheared toroidal flow in tokamak plasmas. *Physics of Plasmas* **18** (10), 102304.
- HIGHCOCK, E. G., BARNES, M., SCHEKOCIHIN, A. A., PARRA, F. I., ROACH, C. M. & COWLEY, S. C. 2010 Transport Bifurcation in a Rotating Tokamak Plasma. *Physical Review Letters* **105** (21), 215003.
- HIGHCOCK, E. G., SCHEKOCIHIN, A. A., COWLEY, S. C., BARNES, M., PARRA, F. I., ROACH, C. M. & DORLAND, W. 2012 Zero-Turbulence Manifold in a Toroidal Plasma. *Physical Review Letters* **109** (26), 265001.
- HOWES, G. G., TENBARGE, J. M., DORLAND, W., QUATAERT, E., SCHEKOCIHIN, A. A., NUMATA, R. & TATSUNO, T. 2011 Gyrokinetic simulations of solar wind turbulence from ion to electron scales. *Physical review letters* **107** (3), 035004.
- JARDIN, S. C., KESSEL, C. E., MAU, T. K., MILLER, R. L., NAJMABADI, F., CHAN, V. S., CHU, M. S., LAHAYE, R., LAO, L. L., PETRIE, T. W., POLITZER, P., ST. JOHN, H. E., SNYDER, P., STAEBLER, G. M., TURNBULL, A. D. & WEST, W. P. 2006 Physics basis for the advanced tokamak fusion power plant, ARIES-AT. *Fusion Engineering and Design* **80** (1-4), 25–62.
- KAWAMORI, E. 2013 Experimental verification of entropy cascade in two-dimensional electrostatic turbulence in magnetized plasma. *Physical review letters* **110** (9), 095001.
- KINSEY, J. E., STAEBLER, G. M., CANDY, J., WALTZ, R. E. & BUDNY, R. V. 2011 ITER predictions using the GYRO verified and experimentally validated trapped gyro-Landau fluid transport model. *Nuclear Fusion* **51** (8), 083001.
- KOTSCHENREUTHER, M., REWOLDT, G. & TANG, W. M. 1995 Comparison of initial value and eigenvalue codes for kinetic toroidal plasma instabilities. *Computer Physics Communications* **88** (2-3), 128–140.
- LEWIS, A. 2004 Parallel Optimisation Algorithms for Continuous, Non-Linear Numerical Simulations. PhD thesis, Griffith University, Brisbane, Australia.
- LUCE, T., CHALLIS, C., IDE, S., JOFFRIN, E., KAMADA, Y., POLITZER, P., SCHWEINZER, J., A.C.C. SIPS, STOBER, J., GIRUZZI, G., KESSEL, C., MURAKAMI, M., NA, Y.-S., PARK, J., A.R. POLEVOI, BUDNY, R., CITRIN, J., GARCIA, J., HAYASHI, N., HOBIRK, J., HUDSON, B., IMBEAUX, F., ISAYAMA, A., McDONALD, D., NAKANO, T., OYAMA, N., PARAIL, V., PETRIE, T., PETTY, C., SUZUKI, T. & WADE, M. 2014 Development of advanced inductive scenarios for ITER. *Nuclear Fusion* **54** (1), 013015.
- LÜTJENS, H., BONDESON, A. & SAUTER, O. 1996 The CHEASE code for toroidal MHD equilibria. *Computer physics communications* **97**, 219–260.
- MAGGI, C. F., GROEBNER, R. J., OYAMA, N., SARTORI, R., HORTON, L. D., SIPS, A. C., SUTTROP, W., LEONARD, A., LUCE, T. C., WADE, M. R., KAMADA, Y., URANO, H., ANDREW, Y., GIROUD, C., JOFFRIN, E. & DE LA LUNA, E. 2007 Characteristics of the H-mode pedestal in improved confinement scenarios in ASDEX upgrade, DIII-D, JET and JT-60U. *Nuclear Fusion* **47** (7), 535–551.
- MANDELL, N. & DORLAND, W. 2014 Hybrid Gyrokinetic/Gyrofluid Simulation of ITG Turbulence. In *Bulletin of the American Physical Society*, p. Abstract CP8.039.
- MANDELL, N., DORLAND, W. & LANDREMAN, M. 2018 Laguerre–hermite pseudo-spectral velocity formulation of gyrokinetics. *Journal of Plasma Physics* **84** (1).
- MANOUSOPOULOS, P. & MICHALOPOULOS, M. 2009 Comparison of non-linear optimization algorithms for yield curve estimation. *European Journal of Operational Research* **192** (2), 594–602.
- MARINONI, A., BRUNNER, S., CAMENEN, Y., CODA, S., GRAVES, J. P., LAPILLONNE, X., POCHELON, A., SAUTER, O. & VILLARD, L. 2009 The effect of plasma triangularity on turbulent transport: modeling TCV experiments by linear and non-linear gyrokinetic simulations. *Plasma Physics and Controlled Fusion* **51** (5), 055016.
- MENEGHINI, O., SNYDER, P. B., SMITH, S. P., CANDY, J., STAEBLER, G. M., BELLI, E. A., LAO, L. L., PARK, J. M., GREEN, D. L., ELWASIF, W., GRIERSON, B. A. & HOLLAND, C. 2016 Integrated fusion simulation with self-consistent core-pedestal coupling. *Physics of Plasmas* **23** (4), 042507.
- MERLE, A., SAUTER, O. & YU MEDVEDEV, S. 2017 Pedestal properties of H-modes with

- negative triangularity using the EPED-CH model. *Plasma Physics and Controlled Fusion* **59** (10).
- MUKHOVATOV, V., SHIMOMURA, Y., POLEVOI, A., SHIMADA, M., SUGIHARA, M., BATEMAN, G., CORDEY, J. G., KARDAUN, O., PEREVERZEV, G., VOITSEKHOVITCH, I., WEILAND, J., ZOLOTUKHIN, O., CHUDNOVSKIY, A., KRITZ, A. H., KUKUSHKIN, A., ONJUN, T., PANKIN, A. & PERKINS, F. W. 2003 Comparison of ITER performance predicted by semi-empirical and theory-based transport models. *Nuclear Fusion* **43** (9), 942–948.
- PARAIL, V., ALBANESE, R., AMBROSINO, R., ARTAUD, J. F., BESSEGHIR, K., CAVINATO, M., CORRIGAN, G., GARCIA, J., GARZOTTI, L., GRIBOV, Y., IMBEAUX, F., KOECHL, F., LABATE, C. V., LISTER, J., LITAUDON, X., LOARTE, A., MAGET, P., MATTEI, M., McDONALD, D., NARDON, E., SAIBENE, G., SARTORI, R. & URBAN, J. 2013 Self-consistent simulation of plasma scenarios for ITER using a combination of 1.5D transport codes and free-boundary equilibrium codes. *Nuclear Fusion* **53** (11), 113002.
- PARKER, J. T., HIGHCOCK, E. G., SCHEKOCIHIN, A. A. & DELLAR, P. J. 2016 Suppression of phase mixing in drift-kinetic plasma turbulence. *Physics of Plasmas* **23** (7), 070703, arXiv: 1603.06968.
- POCHELON, A., ANGELINO, P., BEHN, R., BRUNNER, S., CODA, S., KIRNEVA, N., MEDVEDEV, S., REIMERDES, H., ROSSEL, J., SAUTER, O., VILLARD, L., WÄGNER, D., BOTTINO, A., CAMENEN, Y., CANAL, G. P., CHATTOPADHYAY, P. K., DUVAL, B. P., FASOLI, A., GOODMAN, T. P., JOLLIET, S., KARPUSHOV, A., LABIT, B., MARINONI, A., MORET, J. M., PITZSCHKE, A., PORTE, L., RANCIC, M. & UDINTSEV, V. S. 2012 Recent TCV results - Innovative plasma shaping to improve plasma properties and insight. *Plasma and Fusion Research* **7** (SPL.ISS.1), 1–8.
- POCHELON, A., GOODMAN, T., HENDERSON, M., ANGIANI, C., BEHN, R., CODA, S., HOFMANN, F., HOGGE, J.-P., KIRNEVA, N., MARTYNOV, A., MORET, J.-M., PIETRZYK, Z. A., PORCELLI, F., REIMERDES, H., ROMMERS, J., ROSSI, E., SAUTER, O., TRAN, M. Q., WEISEN, H., ALBERTI, S., BARRY, S., BLANCHARD, P., BOSSHARD, P., CHAVAN, R., DUVAL, B. P., ESIPCHUCK, Y. V., FASEL, D., FAVRE, A., FRANKE, S., FURNO, I., GORGERAT, P., ISOZ, P.-F., JOYE, B., LISTER, J., LLOBET, X., MAGNIN, J.-C., MANDRIN, P., MANINI, A., MARLÉTAZ, B., MARMILLOD, P., MARTIN, Y., MAYOR, J.-M., MLYNAR, J., NIESWAND, C., PARIS, P., PEREZ, A., PITTS, R., RAZUMOVA, K., REFKE, A., SCAVINO, E., SUSHKOV, A., TONETTI, G., TROYON, F., TOLEDO, W. V. & VYAS, P. 1999 Energy confinement and MHD activity in shaped TCV plasmas with localized electron cyclotron heating. *Nuclear Fusion* **39** (11Y), 1807–1818.
- ROACH, C., WALTERS, M., BUDNY, R., IMBEAUX, F., FREDIAN, T., GREENWALD, M., STILLERMAN, J., ALEXANDER, D., CARLSSON, J., CARY, J., RYTER, F., STOBER, J., GOHIL, P., GREENFIELD, C., MURAKAMI, M., BRACCO, G., ESPOSITO, B., ROMANELLI, M., PARAIL, V., STUBBERFIELD, P., VOITSEKHOVITCH, I., BRICKLEY, C., FIELD, A., SAKAMOTO, Y., FUJITA, T., FUKUDA, T., HAYASHI, N., HOGEWELJ, G., CHUDNOVSKIY, A., KINERVA, N., KESSEL, C., ANIEL, T., HOANG, G., ONGENA, J., DOYLE, E., HOULBERG, W. & POLEVOI, A. 2008 The 2008 Public Release of the International Multi-tokamak Confinement Profile Database. *Nuclear Fusion* **48** (12), 125001.
- ROGERS, B. N., DORLAND, W. & KOTSCHENREUTHER, M. 2000 Generation and stability of zonal flows in ion-temperature-gradient mode turbulence. *Physical review letters* **85** (25), 5336–9.
- ROSENBLUTH, M. & HINTON, F. 1998 Poloidal flow driven by ion-temperature-gradient turbulence in tokamaks. *Physical review letters* **80** (4), 724.
- SCHEKOCIHIN, A. A., COWLEY, S. C., DORLAND, W., HAMMETT, G. W., HOWES, G. G., QUATAERT, E. & TATSUNO, T. 2009 Astrophysical Gyrokinetics: Kinetic and Fluid Turbulent Cascades in Magnetized Weakly Collisional Plasmas. *The Astrophysical Journal Supplement Series* **182** (1), 310–377.
- SCHEKOCIHIN, A. A., PARKER, J. T., HIGHCOCK, E. G., DELLAR, P. J., DORLAND, W. & HAMMETT, G. W. 2016 Phase mixing versus nonlinear advection in drift-kinetic plasma turbulence. *Journal of Plasma Physics* **82** (02), 905820212, arXiv: 1508.05988.
- SIMPSON, T., TOROPOV, V., BALABANOV, V. & VIANA, F. 2008 Design and Analysis of Computer Experiments in Multidisciplinary Design Optimization: A Review of How Far We Have Come - Or Not. *12th AIAA/ISSMO Multidisciplinary Analysis and Optimization Conference* (September), 1–22.

- SNYDER, P. & HAMMETT, G. 2001 A Landau fluid model for electromagnetic plasma microturbulence. *Physics of Plasmas* **8** (7), 3199–3216.
- SORBOM, B. N., BALL, J., PALMER, T. R., MANGIAROTTI, F. J., SIERCHIO, J. M., BONOLI, P., KASTEN, C., SUTHERLAND, D. A., BARNARD, H. S., HAAKONSEN, C. B., GOH, J., SUNG, C. & WHYTE, D. G. 2015 ARC: A compact, high-field, fusion nuclear science facility and demonstration power plant with demountable magnets. *Fusion Engineering and Design* **100**, 378–405, arXiv: 1409.3540.
- STAEBLER, G. M. & JOHN, H. E. S. 2006 Predicted toroidal rotation enhancement of fusion power production in ITER. *Nuclear Fusion* **46** (8), L6–L8.
- STAEBLER, G. M., KINSEY, J. E. & WALTZ, R. E. 2007 A theory-based transport model with comprehensive physics. *Physics of Plasmas* **14** (5).
- STORK, D., AGOSTINI, P., BOUTARD, J. L., BUCKTHORPE, D., DIEGELE, E., DUDAREV, S. L., ENGLISH, C., FEDERICI, G., GILBERT, M. R., GONZALEZ, S., IBARRA, A., LINSMEIER, C., PUMA, A. L., MARBACH, G., PACKER, L. W., RAJ, B., RIETH, M., TRAN, M. Q., WARD, D. J. & ZINKLE, S. J. 2014 Materials R&D for a timely DEMO: Key findings and recommendations of the EU Roadmap Materials Assessment Group. *Fusion Engineering and Design* **89** (7-8), 1586–1594.
- SUGAMA, H. & HORTON, W. 1998 Nonlinear electromagnetic gyrokinetic equation for plasmas with large mean flows. *Physics of Plasmas* **5** (7), 2560.
- SYNAKOWSKI, E. J. 1999 Formation and structure of internal and edge transport barriers. *Plasma Physics and Controlled Fusion* **40** (5), 581–596.
- TATSUNO, T., DORLAND, W., SCHEKOCIHIN, A. A., PLUNK, G. G., BARNES, M., COWLEY, S. C. & HOWES, G. G. 2009 Nonlinear phase mixing and phase-space cascade of entropy in gyrokinetic plasma turbulence. *Physical Review Letters* **103** (1), 2–5, arXiv: 0811.2538.
- TATSUNO, T., PLUNK, G., BARNES, M., DORLAND, W., HOWES, G. & NUMATA, R. 2012 Freely decaying turbulence in two-dimensional electrostatic gyrokinetics. *Physics of Plasmas* **19** (12), 122305.
- UCKAN, N. 1990 ITER physics design guidelines: 1989. In *ITER Documentation Series 10* (Vienna: IAEA).
- WAGNER, F., FUSSMANN, G., GRAVE, T., KEILHACKER, M., KORNHERR, M., LACKNER, K., MCCORMICK, K., MÜLLER, E. R., STÄBLER, A., BECKER, G., BERNHARDI, K., DITTE, U., EBERHAGEN, A., GEHRE, O., GERHARDT, J., GIERKE, G. V., GLOCK, E., GRUBER, O., HAAS, G., HESSE, M., JANESCHITZ, G., KARGER, F., KISSEL, S., KLÜBER, O., LISITANO, G., MAYER, H. M., MEISEL, D., MERTENS, V., MURMANN, H., POSCHENRIEDER, W., RAPP, H., RÖHR, H., RYTER, F., SCHNEIDER, F., SILLER, G., SMEULDERS, P., SÖLDNER, F., SPETH, E., STEUER, K. H., SZYMANSKI, Z. & VOLLMER, O. 1984 Development of an Edge Transport Barrier at the H-Mode Transition of ASDEX. *Physical Review Letters* **53** (15), 1453–1456.
- WEISEN, H., ALBERTI, S., BERRY, S., BEHN, R., BLANCHARD, P., BOSSHARD, P., BÜHLMANN, F., CHAVAN, R., CODA, S., DESCHENAUX, C., DUTCH, M. J., DUVAL, B. P., FASEL, D., FAVRE, A., FRANKE, S., FURNO, I., GOODMAN, T., HENDERSON, M., HOFMANN, F., HOGGE, J.-P., ISOZ, P.-F., JOYE, B., LISTER, J. B., LLOBET, X., MAGNIN, J.-C., MANDRIN, P., MARLETAZ, B., MARMILLOD, P., MARTIN, Y., MAYOR, J.-M., MORET, J.-M., NIESWAND, C., PARIS, P., PEREZ, A., PIETRZYK, Z. A., PIFFL, V., PITTS, R. A., POCHOLON, A., RAZUMOVA, K., REIMERDES, H., REFKE, A., ROMMERS, J., ROY, I., SAUTER, O., SUTTROP, W., TOLEDO, W. V., TONETTI, G., TRAN, M. Q., TROYON, F., VYAS, P. & WARD, D. J. 1999 Effect of plasma shape on confinement and MHD behaviour in TCV. *Plasma Physics and Controlled Fusion* **39** (12B), B135–B144.
- WENNINGER, R., ARBEITER, F., AUBERT, J., AHO-MANTILA, L., ALBANESE, R., AMBROSINO, R., ANGIANI, C., ARTAUD, J.-F., BERNERT, M., FABLE, E., FASOLI, A., FEDERICI, G., GARCIA, J., GIRUZZI, G., JENKO, F., MAGET, P., MATTEI, M., MAVIGLIA, F., POLI, E., RAMOGIDA, G., REUX, C., SCHNEIDER, M., SIEGLIN, B., VILLONE, F., WISCHMEIER, M. & ZOHN, H. 2015 Advances in the physics basis for the European DEMO design. *Nuclear Fusion* **55**, 063003.
- WHITE, A. E., HOWARD, N. T., GREENWALD, M., REINKE, M. L., SUNG, C., BAEK, S., BARNES, M., CANDY, J., DOMINGUEZ, A., ERNST, D., GAO, C., HUBBARD, A. E., HUGHES, J. W., LIN, Y., MIKKELSEN, D., PARRA, F. I., PORKOLAB, M., RICE, J. E., WALK, J., WUKITCH, S. J. & TEAM, A. C.-M. 2013 Multi-channel transport experiments

- at Alcator C-Mod and comparison with gyrokinetic simulations. *Physics of Plasmas* **20** (5), 056106.
- VAN WYK, F., HIGHCOCK, E. G., SCHEKOCHIHIN, A. A., ROACH, C. M., FIELD, A. R. & DORLAND, W. 2016 Transition to subcritical turbulence in a tokamak plasma. *Journal of Plasma Physics* **82** (6), arXiv: 1607.08173.
- XANTHOPOULOS, P., MYNICK, H. E., HELANDER, P., TURKIN, Y., PLUNK, G. G., JENKO, F., GÖRLER, T., TOLD, D., BIRD, T. & PROLL, J. H. 2014 Controlling turbulence in present and future stellarators. *Physical Review Letters* **113** (15), 1–4.
- XIAO, Y., CATTO, P. J. & DORLAND, W. 2007 Effects of finite poloidal gyroradius, shaping, and collisions on the zonal flow residual. *Physics of plasmas* **14** (5), 055910.
- ZOHM, H., ANGIONI, C., FABLE, E., FEDERICI, G., GANTENBEIN, G., HARTMANN, T., LACKNER, K., POLI, E., PORTE, L., SAUTER, O., TARDINI, G., WARD, D. & WISCHMEIER, M. 2013 On the physics guidelines for a tokamak DEMO. *Nuclear Fusion* **53** (7), 073019.